

**DEVELOPMENT AND CHARACTERIZATION OF TIC OHMIC
CONTACTS FOR N-TYPE SIC**

Ajay Kumar Chaddha

B.Tech., Regional Engineering College, Rourkela, India, 1989

M.S., Oregon Graduate Institute of Science & Technology, Portland, Oregon 1994

A dissertation submitted to the faculty of the
Oregon Graduate Institute of Science & Technology
in partial fulfillment of the
requirements for the degree
Doctor of Philosophy
in
Materials Science

February 1997

The dissertation "Development and Characterization of TiC Ohmic Contacts for n-type SiC" by Ajay K. Chaddha has been examined and approved by the following Examination Committee:

 James D. Parsons, Advisor
Associate Professor 

William E. Wood
Professor

David Atteridge
Professor

Margaret Ziomek-Moroz
Assistant Professor

 David R. Evans
Sharp Microelectronics, Inc.

To My Parents

ACKNOWLEDGEMENTS

First and foremost the author would like to thank his advisor, Dr. James D. Parsons for his able guidance, support and encouragement during this research work. Many thanks are also due to Dr. Dave Evans for the technical support and for examining this dissertation along with Dr. William E. Wood, Dr. David Atteridge, Dr. Margaret Ziomek-Moroz.

I also gratefully acknowledge the Wright Laboratories for their sponsorship of this research under contract no. F33615-92-C-5959 and F33615-93-C-1345.

My deep thanks to a Gregg Kruaval without whose invaluable technical support and service this dissertation would not have been possible.

I extend many thanks to my fellow students Jin Wu, Karen Oatis, Sukryong Hahn, H.S. Chen, Shafqat Ahmed, Ganta Prasanna, Daya Singh and others in both EEAP and MSE departments for their help and friendship, making my stay at OGI an enjoyable one.

TABLE OF CONTENTS

DEDICATION.....	iii
ACKNOWLEDGEMENTS.....	iv
TABLE OF CONTENTS.....	v
LIST OF TABLES.....	viii
LIST OF FIGURES.....	ix
ABSTRACT.....	xi
CHAPTER 1	
INTRODUCTION.....	1
CHAPTER 2	
LITERATURE REVIEW OF SiC DEVICE TECHNOLOGY.....	4
2.1. CRYSTAL STRUCTURE OF SiC.....	4
2.2. SiC AS A SEMICONDUCTOR.....	6
2.2.1. HIGH TEMPERATURE, CORROSION RESISTANT PROPERTIES.....	6
2.2.2. HIGH POWER, HIGH FREQUENCY, HIGH SPEED PROPERTIES.....	8
2.3. SiC SYNTHESIS.....	11
2.3.1. BULK CRYSTAL GROWTH.....	11
2.3.2. THIN FILM GROWTH.....	12
2.4. HISTORICAL REVIEW OF SiC OHMIC CONTACT TECHNOLOGY.....	15

CHAPTER 3

SINGLE CRYSTAL SiC THIN FILM SYNTHESIS	17
3.1. MOCVD SYSTEM DESIGN AND CONSTRUCTION.....	17
3.2. β -SiC THIN FILM SYNTHESIS.....	24
3.2.1. TITANIUM CARBIDE SUBSTRATE FOR β -SiC EPITAXIAL GROWTH	24
3.2.2. TiC _x SUBSTRATE PREPARTION PROCEDURE	26
3.2.3. GENERAL PROCEDURE FOR GROWTH	27
3.2.4. OPTIMIZATION OF GROWTH USING 1,2-DISILYLETHANE	28
3.1. 6H α -SiC THIN FILM SYNTHESIS	34
3.2. IN-SITU DOPING OF SiC EPILAYERS	34
3.3. SUMMARY	35

CHAPTER 4

TIC AS A OHMIC CONTACT METAL & CONTACT FORMATION PROCESSES	36
4.1. SELECTION OF OHMIC CONTACT METAL.....	36
4.2. CHOICE OF METHODS FOR OHMIC CONTACT DEPOSITION	38
4.3. EPITAXIAL TIC DEPOSITION BY MOCVD	38
4.4. POLYCRYSTALLINE TIC DEPOSITION.....	41
4.4.1. SPUTTER DEPOSITION METHOD	41
4.4.2. SPUTTER DEPOSITION APPARATUS & EXPERIMENTAL PROCEDURE.....	46
4.5. SUMMARY	53

CHAPTER 5

CHARACTERIZATION METHODS & PROCEDURES FOR TIC OHMIC CONTACTS	54
5.1. MEASUREMENT OF SPECIFIC OHMIC CONTACT RESISTANCE.....	54

5.1.1. THEORY OF MEASUREMENT TECHNIQUE	55
5.1.2. FABRICATION OF TLM STRUCTURES.....	59
5.1.3. MEASUREMENT PROCEDURE	63
5.2. DETERMINATION OF STABILITY OF CVD TiC/SiC INTERFACE.....	63
5.3. TEST OF HARDNESS AND ADHESION	64
CHAPTER 6	
RESULTS & DISCUSSION OF OHMIC CONTACT CHARACTERIZA-	
TION.....	67
6.1. MEASUREMENT OF SPECIFIC OHMIC CONTACT RESISTANCE.....	67
6.1.1. RESULTS AND DISCUSSION	67
6.2. DETERMINATION OF STABILITY OF TIC/SIC INTERFACE	82
6.2.1. RESULTS AND DISCUSSION	82
6.3. RESULTS OF TEST OF HARDNESS AND ADHESION	82
CHAPTER 7	
CONCLUSIONS.....	84
7.1. CONCLUSIONS	84
7.2. ACKNOWLEDGEMENTS	85
REFERENCES.....	86
VITA	98

LIST OF TABLES

Table 2.1: Selected SiC Polytypes.....	5
Table 2.2: Comparison of important electronic properties of β -SiC, 6H α -SiC, Si and GaAs.	10
Table 2.3: Specific ohmic contact resistance of some metal systems reported in literature.	16
Table 3.1: Selected reactant sources in β -SiC MOCVD system.	19
Table 3.2: Physical Properties of β -SiC and TiC.....	25
Table 6.1: Dimensions obtained after fabrication of TLM structures.	68
Table 6.2: Transfer length measurement data and calculations (CVD TiC/ n ⁺ 6H α -SiC).....	76
Table 6.3: Transfer length measurement data and calculations (sputtered TiC/ n ⁺ 6H α -SiC).	77
Table 6.4: Transfer length measurement data and calculations (CVD TiC/ n ⁺ β -SiC).....	78

LIST OF FIGURES

Fig. 3.1. Schematic diagram of β -SiC MOCVD system.....	22
Fig. 3.2. Cross-sectional view of inverted-vertical CVD reactor.....	23
Fig. 3.3. Nomarsky photographs (30X) of a polished TiC substrate	31
Fig. 3.4. Optimized thermal cycle for β -SiC growth on titanium carbide substrate. ...	31
Fig. 3.5. S.E.M micrographs of polished β -SiC grown under optimized conditions (a) and unoptimized conditions (b).....	32
Fig. 3.6. SEM cross section of β -SiC/TiC interface for growth rate determination. ...	33
Fig. 3.7. Electron channeling contrast pattern from (111) β -SiC epilayer.....	33
Fig. 4.1. SEM micrograph of a TiC epilayer grown on 6H α -SiC.....	40
Fig. 4.2. Electron channeling contrast pattern from a TiC epilayer grown on (0001) 6H α -SiC.....	40
Fig. 4.3. Idealized view of a source and a substrate mounted on a sphere.	44
Fig. 4.4. Cross-section view of the 5 inch S-gun (courtesy Varian assoc.).	47
Fig. 4.5. TiC sputter deposition rate versus power at constant gas pressure of 15 ± 1 millitorr.....	51
Fig. 4.6. TiC sputter deposition rate versus sputtering gas pressure at constant power of 1000 ± 15 W.....	52

Fig. 5.1. A transfer length method test structure with dimensions and a plot of total resistance as a function of contact spacing d.	59
Fig. 5.2. Process steps for fabrication of TLM structures.....	65
Fig. 5.2. Process steps for fabrication of TLM structures.....	66
Fig. 6.1. TLM structure on (a) sample A, (b) sample B and (c) sample C, showing TiC Shockley pads; light areas are TiC, dark area is n ⁺ SiC.	73
Fig. 6.2. TiC Shockley pad dimensions and mesa width on (a) sample A, (b) sample B (annealed) and (c) sample C.....	74
Fig. 6.3. Equilibrium band diagram of ideal TiC/n-SiC (degenerately doped) accumulation type ohmic contact.....	75
Fig. 6.4. Average resistance between Shockley pads versus spacing for CVD TiC/n-type 6H α -SiC.....	79
Fig. 6.5. Average resistance between Shockley pads versus spacing for sputtered TiC/n-type 6H α -SiC.....	80
Fig. 6.6. Average resistance between Shockley pads versus spacing for CVD TiC/n-type β -SiC.....	81
Fig. 6.7. XTEM micrographs showing (a) epitaxial CVD TiC/6H α -SiC interface and (b) epitaxial CVD TiC/ β -SiC interface.....	83

ABSTRACT

DEVELOPMENT AND CHARACTERISATION OF TiC OHMIC CONTACTS FOR N-TYPE SiC

Ajay K. Chaddha, Ph.D

Supervising Professor: James D. Parsons

TiC ohmic contact metallization to n-type β -SiC and $6H\alpha$ -SiC was developed and characterized. TiC was deposited using dc sputtering and chemical vapor deposition.

A metal-organic chemical vapor deposition (MOCVD) system, with an inverted vertical reactor, was designed and built. A MOCVD process using a single reactant source (1,2-disilylethane or $\text{Si}_2\text{C}_2\text{H}_{10}$) was optimized and used to grow single crystal SiC on TiC substrates. The epilayers had a smooth morphology and were free of double positioning boundaries, antiphase domains and stacking faults. NH_3 was used for in-situ nitrogen doping. In-situ B doping for isolation layers was achieved by B_2H_6 . Epitaxial CVD TiC was grown on SiC using TiCl_4 and C_2H_4 sources. Sputtering system was built and TiC sputter deposition was developed.

Transfer length method was used to measure the specific contact resistance (ρ_c), sheet resistance of n-type SiC (ρ_s) and contact resistance (R_c) of TiC ohmic

contacts. TLM test structures were fabricated using photolithography, reactive ion etching (SF_6) and wet etching.

The ρ_c values obtained are the lowest ever reported for ohmic contacts to n-type SiC. Average ρ_c obtained for epitaxial TiC contacts on n^+ ($4 \times 10^{19} \text{ cm}^{-3}$) 6H α -SiC was $1.30 \times 10^{-5} \Omega \cdot \text{cm}^2$ and for sputtered TiC contacts = $2.89 \times 10^{-5} \Omega \cdot \text{cm}^2$. The $\approx 55\%$ lower ρ_c for epitaxial contacts compared to that of sputtered contacts suggests that epitaxial ohmic contacts are more ideal Schottky barriers. For epitaxial TiC contacts on n^+ ($2 \times 10^{19} \text{ cm}^{-3}$) β -SiC, ρ_c was $5.44 \times 10^{-6} \Omega \cdot \text{cm}^2$ which is 60% lower than for CVD TiC/ n^+ 6H α -SiC contacts. The comparative value is in accordance with superior transport properties of β -SiC.

Cross-sectional transmission electron microscopy of CVD TiC/SiC interface did not show presence any third phases or interdiffusion. Contact resistance remained unaffected after subjecting the contacts to high current density conditions for one hour. Excellent hardness and adhesion was shown by all contacts.

CHAPTER 1

INTRODUCTION

The potential of SiC semiconductor for high power, high temperature and high frequency applications in electronics is well recognized.¹⁻⁶ Owing to its superior electronic properties it can out perform semiconducting materials currently in use.

However, the SiC device technology development is still in its infancy. Significant progress in single crystal synthesis and device processing has been made in recent years,^{7,8} especially in case of 6H α -SiC. High quality bulk grown 6H α -SiC single crystals are now commercially available which can be used for homo-epitaxial chemical vapor deposition of 6H α -SiC thin films.¹² The same is not true for β -SiC. Hetero-epitaxial chemical vapor deposited β -SiC thin films grown on Si and 6H α -SiC substrates continue to be plagued by high defect densities. A large part of the problem is the choice of substrates, namely Si and 6H α -SiC. On the other hand, Parsons et al.^{15-17,72} have developed β -SiC thin film synthesis by chemical vapor deposition on TiC substrate and this approach has shown most promise thus far. β -SiC epitaxial growth on TiC substrate comes very close to a lattice matched growth and hence yields epilayers with significantly lower defect densities.

On the device processing front of the technology development, development of ohmic contact metallization for the semiconductor is critically important. The requirements in case of SiC are particularly stringent because not only do the ohmic contact resistances have to be very low (for high frequency device operation) but they also must be stable at high temperature and high power (high current density) conditions. Most important power devices require only n-type ohmic contacts, therefore considerable effort is presently devoted to exploring n-type SiC ohmic contact materials, contact formation processes and contact/SiC interface properties.^{93,96-104,112} The lowest reported specific contact resistances to n-type SiC^{97-101,112} are greater than $10^{-4} \Omega \cdot \text{cm}^2$. Specific contact resistances of the order of $10^{-5} \Omega \cdot \text{cm}^2$ are desired for operation of gigahertz frequency range SiC circuits.

The need for a contact metal to completely meet all the requirements of ohmic contacts for n-type SiC, led to the objective of this research work to investigate and develop TiC ohmic contact metallization for n-type SiC. The work was accomplished using following major steps:

(1) Optimization of β -SiC and $6H\alpha$ -SiC epitaxial growth by metal-organic chemical vapor deposition (MOCVD) on TiC and $6H\alpha$ -SiC substrates respectively. This step was necessary because good quality single crystal SiC thin films were needed to form the contact layers for the ohmic contacts.

(2) Sputter deposition and chemical vapor deposition of TiC on β -SiC and $6H\alpha$ -SiC. These were the two contact formation processes selected for TiC ohmic contact metallization.

(3) Measurement of specific contact resistance¹⁰⁶ (contact resistance per unit

area) of the TiC ohmic contacts deposited by the two contact formation processes. In order to do the measurements, Transfer length measurement (TLM) structures were fabricated on which the measurements were performed.

(4) Comparison of the results of specific contact resistance measurements, i.e sputter deposited ohmic contacts versus chemical vapor deposited, and ohmic contacts to β -SiC versus ohmic contacts to $6H\alpha$ -SiC.

(5) Determination of hardness and adhesion of TiC contacts, and determination of stability of TiC/SiC interface. The interface stability was evaluated by two methods. First, by cross-section transmission electron microscopy of chemical vapor deposited TiC/SiC interfaces (effect of high temperature) and second, by subjecting the ohmic contacts to high current density conditions for long duration.

This dissertation is organized into seven chapters including this introduction. Chapter 2 contains a literature review of SiC device technology, including its advantages as a semiconducting material, recent progress in research and the main hurdles facing SiC device technology development. Chapter 3 discusses the approach taken for single crystal SiC synthesis and results of process optimization. The choice of TiC to form ohmic contacts to n-type SiC, the selection of contact formation processes, and the processes that were developed, are described in chapter 4. Chapter 5 presents the methods and procedures used to characterize the TiC ohmic contacts. Results and discussion of ohmic contact characterization constitute chapter 6. Conclusions are presented in chapter 7.

CHAPTER 2

LITERATURE REVIEW OF SiC DEVICE TECHNOLOGY

The unique thermal and electronic properties of silicon carbide have been known since early 1950's. These properties have lead to one of the highest figures of merit¹⁻³ for any semiconductor material for use in high power, high speed, high temperature, high frequency and radiation hard applications. SiC synthesis was a bottleneck to any rapid progress in the development of SiC electronics for a long duration. Only in recent years has the development of SiC device technology been given a new impetus by significant advances in SiC synthesis.^{13-15,17} This chapter reviews these recent developments along with the properties which make this semiconductor so promising for afore-mentioned applications.

2.1. CRYSTAL STRUCTURE OF SiC

Silicon carbide is the only stable compound species that exists in the solid state in the Si-C system. It has four known polymorphs with the following crystal structures:²⁰⁻²² cubic (C), hexagonal (H), rhombohedral (R), and trigonal (T). The cubic form crystallizes in a zincblende (ZnS) structure and is known as 3C-SiC or β -SiC. The rest of the crystal structures are collectively referred to as α -SiC.

SiC, a close-packed structure, exhibits an unusual phenomenon of

polytypism.^{21,23} Polytypism can be called a one dimensional polymorphism. Polytypes are alike in the two dimensions of the close packed planes but differ in the stacking sequence in the direction perpendicular to these planes. In SiC, a specific polytype is identified according to the stacking sequence of double layers of Si and C atoms. Each double layer consists of close-packed Si over a close-packed C. This double layer is actually a close packed plane of covalently bonded primary coordination tetrahedra (either SiC₄ or CSi₄). Only three possible relative positions for the double layers are allowed in a close-packed stacking arrangement, denoted by A, B, C. The stacking sequence for β -SiC is that of a face centered cubic, i.e. ABC. The rest of the crystal structures (α -SiC) have a simple hexagonal stacking sequence ABAB or more a complex, wider range, larger period stacking sequence. More than 250 stacking sequences and hence polytypes have been identified in α -SiC.²⁴ Some common SiC polytypes are listed in Table 2.1. In the notation of each polytype, the number preceding the crystal structure designator (C, H or R) is the number of double layers in a stacking repeat sequence.

Table 2.1: Selected SiC Polytypes.

	Notation	Stacking Sequence
Cubic or Beta	3C	ABCABC...
Alpha	2H	ABAB...
	4H	ABACABAC...
	6H	ABCACBABCACB...
	15R	ABCBACABACBCACB...

Different polytypes have similar physicochemical properties but offer a wide range of band gap energies (from 2.4 eV to 3.3 eV) and differ in other electrical properties.²⁵ This increases SiC's versatility giving rise to interesting different applications from electronics viewpoint.

2.2. SiC AS A SEMICONDUCTOR

β -SiC, because of its unique properties, is the best candidate for meeting the future semiconductor device and integrated circuit requirements, namely

- (1) higher operating temperatures
- (2) higher power outputs
- (3) higher operating frequencies
- (4) high speed integrated circuits
- (5) greater resistance to radiation damage

2.2.1. HIGH TEMPERATURE, CORROSION RESISTANT PROPERTIES

Si electronics start to fail in hostile environments. Most corrosive gas species etch or easily diffuse into Si at temperatures as low as 100 °C. It becomes impossible to use Silicon above 300 °C for extended periods of time because of movement of dopant impurities. SiC on the other hand has very low diffusion coefficients of dopant impurities and is an extremely inert material, that can only be etched by molten alkalis or chlorine and hydrogen gases at high temperatures.

The properties considered to be most important for high temperature semiconductor applications are: (1) Band gap energy, (2) chemical stability, (3)

Debye temperature, (4) density, (5) fractional ionic character of interatomic bonds.

Wide band gap semiconducting materials are less susceptible to thermal excitation of charge carriers by internal or external heating and hence less susceptible to thermal runaway.

Chemical stability is of primary importance because it is essential that the semiconductor does not decompose or undergo a phase transformation at operating temperatures. High bond strength of Si-C bond (≈ 5 eV) causes high chemical stability in SiC.

The Debye temperature is that temperature at which virtually all lattice modes are oscillating at maximum or Debye frequency (ν_D) for a particular crystal lattice. This parameter is important, because as the distribution of lattice frequencies approaches ν_D , the electronic transport properties deteriorate due to increased collisions between charge carriers and the crystal lattice. The Debye temperature for SiC is at least double than that for Si and GaAs (Table 2.2).

Density can be considered as a qualitative measure of resistance to diffusion of foreign atoms in the lattice. Dopant atoms are less likely to move in a dense crystal. SiC has a high density of 3.21 g/cm^3 whereas Si has a density of 2.32 g/cm^3 , at $300 \text{ }^\circ\text{K}$.

The fractional ionic character of the interatomic bonds is very important for semiconductor device applications. The donor electrons and acceptor holes become more tightly bound as the fractional ionic character of the bonds in a crystal increases. This gives rise to poor electronic transport properties and increases the voltages required to move current. The ultimate effect of increasing the fraction of

ionic bonding is that the voltages required to free electrons and holes from donor and acceptor atoms, respectively, are also sufficient to free electrons from host atoms and to move ions. In this worst case scenario the material would become conductive. SiC has a acceptable fractional ionic character of 0.18 and Si of 0.00.

2.2.2. HIGH POWER, HIGH FREQUENCY, HIGH SPEED PROPERTIES

SiC is not only suitable for high temperature, corrosion resistant semiconductor requirements but also has an excellent potential for: (1) higher power outputs, (2) higher operating frequencies, and (3) increased device packing density. The key properties responsible for such performance are: (1) large band gap, (2) high breakdown electric field, (3) high thermal conductivity, (4) low dielectric constant, (5) high saturated drift velocity, and (6) high low field mobility (Table 2.2).

As stated earlier, large band gap semiconducting materials are less susceptible to thermal runaway. This enables them to operate at higher power levels and handle higher current densities because the heat dissipated due to joule effect does not degrade performance. Also, they usually possess high breakdown electric field. This parameter has dual importance in power devices. Its primary importance in power switches is to maximize the reverse blocking voltage or to reduce the channel thickness required to block a given voltage. In high frequency power FET's, it allows one to reduce the device dimension for a given power output and thus increases maximum operating frequency.

Thermal conductivity (σ_t) is a limiting factor in the duty cycle and maximum

packing density of high frequency, high power devices. SiC has σ_t equivalent to that of copper at room temperature, unlike any other semiconductors. In qualitative terms, SiC can dissipate 3.3 times more power than Si and 10 times more power GaAs for the same amount of cooling.

The dielectric constant (κ), the ratio of permittivity of the semiconductor to the permittivity of free space, is important to high frequency device operation through its effect on the dielectric relaxation time. This is because the amount of charge to set a given potential is directly proportional to κ . A low κ value, as is in the case of SiC, also results in lower parasitic capacitances, and a smaller impedance per unit device area. This means a smaller transistor can drive the same electrical signal and device size reduction can be achieved.

The maximum frequency of operation for a transistor is decided by the minimum charge transit time from the point of injection to the point of collection. The charge transit time depends on the low field mobility and saturated drift velocity of the carriers. β -SiC has a mobility value comparable to that of Si whereas $6H\alpha$ -SiC has lower mobility value. This is because β -SiC has higher symmetry than α -SiC and reduced phonon scattering. The reported values of mobility for SiC in Table 2.2 have considerable uncertainty because of variation in material quality. An important fact here is that SiC has a higher Debye temperature than Si or GaAs which means that it will experience much less mobility reduction per degree rise in temperature.

Small devices generally operate at higher electrical fields where the maximum operating frequency depends on the saturated drift velocity (V_{sat}). The

V_{sat} value for β -SiC determined by Parsons et al. lies between 2.0×10^7 cm/s and 2.5×10^7 cm/s,³⁵ whereas the theoretically predicted value is approximately 2.5×10^7 cm/s.³⁶ $6H\alpha$ -SiC has a slightly lower value of 2.0×10^7 cm/s⁴⁶ due to higher phonon scattering. Both values are superior to those of GaAs and Si.

Table 2.2: Comparison of important electronic properties of β -SiC, $6H\alpha$ -SiC, Si and GaAs.

Properties	Units	β -SiC	$6H\alpha$ -SiC	Si	GaAs	Reference
Bandgap Energy	eV	2.35	2.86	1.12	1.43	26-28
N-type Dopant E_d	meV	20	63	39	6	28-30
P-type Dopant E_a	meV	160	210	45	26	28,30,32, 33
Drift mobility (Electrons)	cm ² V-s	> 800	≤ 400	1380	8500	28,34,36
Drift mobility (Holes)	cm ² /V-s	?	?	495	400	28,34
Hall mobility (Electrons)	cm ² /V-s	750- 4670	400-607	1500	9000	28,31,37- 42
Hall mobility (Holes)	cm ² /V-s	50-650	50	450	450	28,42,43
Breakdown Electric Field E_B	V/cm	$> 5 \times 10^6$	$> 5 \times 10^6$	3×10^5	4×10^5	28,44
Saturated Drift Velocity (e^-) v_s	cm/s	2.5×10^7	2×10^7	1×10^7	2×10^7	28,36,37, 45,46
Dielectric Constant $\kappa (\epsilon_s/\epsilon_0)$		9.7	≥ 9.7	11.8	12.8	47
Thermal Conductivity σ_t	W/cm °K	4.9	4.9	1.5	0.5	48
Debye Temperature	°K	1430	1270	636	360	20,50,51

2.3. SiC SYNTHESIS

High performance devices require semiconductor material with good crystallinity, very low defect density and background carrier concentration. The difficulty in producing such high quality material has been the main obstacle in SiC device technology development. The following subsections give a review of recent developments in bulk crystal and thin film synthesis of SiC.

2.3.1. BULK CRYSTAL GROWTH

Commonly used methods of growing and purifying bulk single crystals, such as melt growth (Czochralski method) and zone refining (Floating-zone method), cannot be used for SiC. This is due to the fact that SiC does not melt, but dissociates at 2830 °C under Ar pressure of 35 atmospheres.⁴⁹ Prior to mid 1950's, SiC was only available from the industrial Acheson process for making abrasive material. In 1955, Lely⁵² reported the development of a sublimation process for growing higher purity α -SiC single crystals. This process met with some success but had problems of uncontrolled nucleation and randomly sized crystals consisting of polytypes. Subsequent research⁹⁻¹¹ has resulted in the implementation of a seeded-growth sublimation process wherein only one large crystal of a single polytype is grown. In this process nucleation occurs on a SiC seed crystal located at top or bottom of cylindrical growth cavity. Similar to Lely process SiC sublimates from a polycrystalline source to form Si, Si₂C and SiC₂ which diffuse through a porous graphite retainer and along carefully programmed thermal and pressure gradients to impinge on the growing crystal.

However, bulk crystal growth of β -SiC by sublimation has been unsuccessful due to the fact β -SiC is unstable above 1600 °C⁵³, much lower than the temperature needed by sublimation process, and tends to convert to α -SiC polytypes.

2.3.2. THIN FILM GROWTH

The reportedly successful vapor phase epitaxy (VPE) approaches consist of growing single crystal β -SiC epilayers by chemical vapor deposition (CVD) or Molecular beam epitaxy (MBE) on Si, 6H α -SiC and TiC substrates. The VPE approach is important for SiC device technology development because it is the only method by which controlled n-type, p-type, and compensation doping have been demonstrated.⁵⁴ In this section the development of these CVD approaches and their utility to β -SiC device technology development will be discussed.

The availability of large area monocrystalline Si in well characterized, reproducible forms of controlled purity spurred its use as a substrate for β -SiC epitaxial growth. β -SiC on Si was first achieved by Nishino et al. in 1983 using a two-step CVD process¹³. Later on this has been duplicated and modified worldwide.⁵⁵⁻⁶⁰

In this approach, first carbonization of Si substrate is achieved via reaction with a carbon containing gas (C₂H₄ or C₃H₈). A “converted layer” or a “buffer layer” forms, on top of which β -SiC thin films are grown using SiH₄ and C₂H₄ or C₃H₈.

The lattice parameter of Si and β -SiC differ by about 20% and coefficients

of thermal expansion by about 8%. Although the purpose of the converted layer is to reduce this mismatch, the layers still have a high defect density. Microstructural analysis via transmission electron microscopy has revealed presence of intrinsic stacking faults, microtwins, misfit dislocations and inversion domain boundaries^{18,19,61} (a.k.a. antiphase boundaries). The density of first two defects is higher at the interface, it decreases over a distance of 3-4 μm and becomes approximately equal to that at the surface even for very thick films. Inversion domain boundaries also extend all the way to the surface of the film. The inversion domain boundaries can be reduced or eliminated by growth on off-axis orientations instead of on-axis orientations.⁸²

Another problem with the β -SiC thin films is heavy compensation. Hall measurements indicate that while net electron carrier concentration in unintentionally doped material is in low 10^{16} cm^3 range, the atomic donor and acceptor concentration are about 10^{18} cm^3 (i.e. $N_A/N_D > 0.9$).^{42,62} The source of compensating acceptors is unknown.

Gas-source MBE of β -SiC on Si has reported β -SiC films nearly as good as those produced via CVD at high temperatures.⁶³

In an attempt to substantially reduce the concentrations of all defects simultaneously, growth on the Si (0001) and C (000 $\bar{1}$) faces of commercial 6H α -SiC single crystals has been investigated.¹⁴ The resulting films were β -SiC (111) with lower defect density. The only significant defects were double positioning boundaries (DPB's) on both Si and C faces.^{64,65}

The occurrence of DPB's can be explained as follows. There are six atoms

on the surface of the hexagonal basal plane to which depositing atoms can bond. If the depositing atoms nucleate as a cubic structure, then there can be only three bonds to the six basal plane atoms. Thus, to form a cubic structure, the nucleating atoms must attach to every other atom in the basal plane of the hexagonal lattice. This results in two equivalent sites (e.g., B and C on plane A in conventional crystal notation in the [111] direction) on a 0001 or a (111) surface. A nucleus forming from an assembly of atoms on A sites will be rotated sixty degrees relative to a nucleus growing on B sites. If the nuclei are incoherent, stacking faults may form to release the internal energy at the boundaries of the nuclei. If these nuclei grow and meet each other, DPB's are formed between them.

The elimination of DPB's was achieved by using vicinal 6H α -SiC substrates (few degrees off the basal plane), but this yielded homo-epitaxial 6H α -SiC layers rather than β -SiC layers.⁶⁶⁻⁶⁸ Powell et al. patterned a 6H α -SiC substrate with 1mm² die-sized areas^{69,70} CVD growth on this substrate produced a mixture of 1mm² β -SiC and 6H α -SiC epilayer mesas. Most β -SiC mesas were DPB free. The stacking fault density was also reduced. However, the distribution of β -SiC mesas versus 6H α -SiC mesas on the wafer was random and uncontrollable. Therefore, this process is not suitable for mass production.

Recently single crystal β -SiC (001) epilayers without DPB's have been reported on 6H α -SiC ($0\bar{1}1\bar{4}$) substrates by Molecular beam epitaxy.⁷¹ The epilayers are grown by alternate supply of disilane (Si₂H₆) and acetylene (C₂H₂) gas molecular beams in high vacuum. These epilayers are also expected to be twinning free because there is no mismatch with 6H α -SiC ($0\bar{1}1\bar{4}$) substrates, but at this time

there is no conclusive evidence that this approach can yield thick, good crystalline quality β -SiC for device applications.

As discussed above, β -SiC epilayers grown on Si and 6H α -SiC fail to adequately meet the requirements for device development technology. Parsons et al. chose TiC as the substrate which has a lattice parameter mismatch to β -SiC of about 0.7% and a cubic crystal structure^{15,72} (rock salt). There is no fundamental limit to minimizing defect densities in β -SiC grown on TiC.

Parsons et al.^{15,17,72,73} demonstrated single crystal β -SiC on TiC by CVD using 1,2-disilylethane as a precursor. Compared to β -SiC films grown on Si and 6H α -SiC substrates, the β -SiC films grown on TiC have much lower defect densities and smoother morphology.

2.4. HISTORICAL REVIEW OF SiC OHMIC CONTACT TECHNOLOGY

As stated in the introduction, the requirements in case of SiC for ohmic contact metallization are particularly stringent because not only do the contact resistances have to be very low, to lower the parasitics in high frequency devices, but they also must be stable at high temperature (600 °C and above) and high power (high current density) conditions.

Refractory metals are preferred for such applications because of their high melting points. These metals also provide better adhesion of contacts because they are prone to form silicides or/and carbides at the interface. However, this can also affect the long term stability of the contacts if the chemical reaction occurs during device operation.

Chromium,⁷⁴ nickel,⁷⁵ titanium,⁷⁶ tantalum,⁷⁸ tungsten,⁷⁶⁻⁷⁸ and molybdenum⁷⁸ are some of the refractory metals which have been studied. Auger electron microscopy studies of Mo/SiC and W/SiC interfaces show that these systems remain stable and change very little even after annealing at temperatures as high as 800 °C and 850 °C respectively.⁷⁸ The Au/W/n-type β -SiC ohmic contact has been reported to have the lowest contact resistance and was found electrically stable at 600 °C.⁷⁶ Au forms rectifying contacts to n-type SiC but degrades into a ohmic contact at 700 °C.⁸¹ It should be remarked that of all the ohmic contact systems studied, none have shown specific contact resistance better than $10^{-4} \Omega \cdot \text{cm}^2$ (Table 2.3). This value is not sufficient to exploit fully the potential advantages of SiC in power microwave devices.

Table 2.3: Specific ohmic contact resistance of some metal systems reported in literature.

Semiconductor	Metal system	Specific contact resistance ($\Omega \cdot \text{cm}^2$)	Ref.
n-type β -SiC	Au/Ta	2×10^{-3}	76
	Au/W	8×10^{-4}	76
	Au/Ti	1×10^{-3}	76
	Au/Ni	2×10^{-3}	75
	W	8×10^{-2}	77
n-type 6H α -SiC	Al/W	1×10^{-4}	79
	Ni, Cr	3×10^{-4}	80

CHAPTER 3

SINGLE CRYSTAL SiC THIN FILM SYNTHESIS

This chapter presents single crystal SiC thin film growth process development and optimization. Following sections constitute this chapter: MOCVD system design and construction description (section 3.1); β -SiC thin film synthesis which includes choice of TiC as a substrate for β -SiC epitaxial growth, TiC substrate preparation procedure, general procedure for growth and method of growth process optimization and its results (section 3.2); 6H α -SiC thin film synthesis (section 3.3); in-situ doping of SiC (section 3.4) and summary (section 3.5).

3.1. MOCVD SYSTEM DESIGN AND CONSTRUCTION

A MOCVD system for β -SiC thin film synthesis was designed and built. The schematic of the system is shown in Fig. 3.1.

Chemical vapor deposition refers to the formation of a condensed phase from a gaseous medium of different chemical composition. The gaseous medium consists of reactant sources and a transport agent. The design of the MOCVD system is dictated by the nature of the reactant sources used in thin film growth. The reactant sources can be either in a gas phase or in a liquid phase. Usually, a gas type

reactant source is contained in a high pressure cylinder, and a liquid source is stored in a stainless steel bubbler, which is kept in a temperature controlled bath to maintain a constant liquid vapor pressure. Hydrogen gas (transport agent) is bubbled through the liquid, which causes it to saturate with the vapor, and then flown to the reactor. The amount of the liquid source transferred, n in moles/min, can be calculated by using the ideal gas equation:

$$n = \frac{RT}{PV} \quad (3.1)$$

where V is the H_2 flow rate in sccm, P is the vapor pressure of the source at the bath temperature, R is the gas constant and T the temperature of bath in °K

The reactant sources installed in our MOCVD system are listed in Table 3.1. β -SiC epitaxial growth was achieved by using a single reactant source 1,2-disilylethane¹¹³ (DSE or $Si_2C_2H_{10}$). Ammonia (NH_3), dimethylaluminum hydride (DMAH or $Al_2C_2H_7$) and diborane (B_2H_6) were selected for *in-situ* doping to produce n-type, p-type and high resistivity β -SiC, respectively. The system also has the ability to grow TiC using $TiCl_4$ and C_2H_4 , and Si using SiH_4 . Epitaxial TiC layer grown on TiC substrate served as a buffer layer in the β -SiC growth process and epilayer grown on n-type SiC was used for ohmic contact metallization studies (see section 4.3). Amongst all the reactant sources, $Si_2C_2H_{10}$, $Al_2C_2H_7$ and $TiCl_4$ are in liquid form, and the others are in gas form.

Table 3.1: Selected reactant sources in β -SiC MOCVD system.

Purpose	β -SiC growth				TiC growth		Si growth
	β -SiC growth	n-type doping	p-type doping	high ρ doping			
Reactant source	Si ₂ C ₂ H ₁₀ (DSE)	NH ₃	Al ₂ C ₂ H ₇ (DMAH)	B ₂ H ₆	TiCl ₄	C ₂ H ₄	SiH ₄
Source type (temp.)	liquid (0 °C)	gas (R.T.)	liquid (15 °C)	gas (R.T.)	liquid (15 °C)	gas (R.T.)	gas (R.T.)

The fundamental requirement for the CVD process is to deliver appropriate reactant sources to the reactor in a controlled manner. Timing and composition of the gaseous phase entering the reactor is the primary determinant of the physical composition and structure of the growing layer. In addition, leak tight integrity of the system is essential when mixing and transporting these reactant sources. Oxygen contamination of the growing film inevitably leads to the degradation of the film properties. Chemically polished 316 stainless steel plumbing is used in the MOCVD system. The chemical polish smoothens and cleans the inner surface of the plumbing. All joints are welded or are high vacuum VCR connections using silver plated gaskets. The system has a leak integrity of better than 10^{-9} cc/min helium. Gas purifiers are installed in all gas lines to reduce impurity concentrations of the gases.

Precise gas flow control is accomplished by using regulators to maintain the gas pressures and using electronic mass flow controllers (MFC) to meter the gas flow rates. As shown in Fig. 3.1, a two-stage regulator is used to control the outlet

pressure of a gas cylinder. The downstream, low pressure stage, is employed to maintain a constant inlet pressure to a MFC which controls gas flow from the gas cylinder to the reactor. In each liquid reactant source line, a second single stage regulator is used in series with the H₂ gas cylinder regulator to control the inlet pressure of the MFC which controls the H₂ flow through the liquid bubbler. The reason for the second regulator is to prevent pressure fluctuations from occurring when two or more liquid source lines are fed by the H₂ carrier gas. The inlet manifold of the system has a run-vent configuration, which allows for development of a steady gas flow to a vent line prior to its introduction into the feed flow to the reactor. During the growth, the appropriate reactive process gases are directed to the feed flow, further diluted by the H₂ carrier, mixed and subsequently introduced into the reactor.

A special feature of the MOCVD system is the water-cooled inverted-vertical (i-v) reactor, as shown in Fig. 3.2. The substrate is placed in the reactor by supporting its growth face downward on a graphite mask which rests on the inside bottom of a high purity pyrolytic boron nitride (PBN) cup or pedestal. The pedestal is co-axially supported within the reactor by a support collar which rests on a pedestal supporting ring fused to the inside wall of the reactor chamber. An induction heated graphite susceptor rests on the top of the back side of the substrate. Two PBN heat shields are mounted over the graphite susceptor, between the susceptor and the pedestal vertical wall, to reduce heat loss. During the growth, carrier gas and gaseous reactant sources enter from the bottom of the reactor. After the reactant source pyrolysis, the gaseous reactant products are pushed radially

outward until they reach the edge of the pedestal where the pressure gradient in the reactor and buoyancy carry the reactant product upwards, through the annular volume between the outer pedestal wall and the inside wall of the reactor chamber. The reactor products exit this volume through the holes at the top of the pedestal, after which they exit through the exhaust port in the reactor cap.

This reactor achieves true stagnation point flow by virtue of the inverted configuration and the orientation of the substrate surface perpendicular to the gas flow direction. At stagnation point flow the fluid flow ceases completely and the mass transport occurs across the stagnant layer by simple diffusion. This is ideal for achieving the best possible uniformity over the largest possible area at atmospheric pressure. Also back-streaming eddies do not form at the growth surface because the buoyancy of the hot gases keeps them in contact with a downward facing surface until they are pushed beyond the radius of that surface and permitted to flow in an upward direction. The buoyancy of the hot gases also causes rapid exhaust^{92,93} of the by-products which makes for a simple reactor design without a need for accessories like a exhaust vacuum pump. Experimental results from GaAs growth using the same reactor configuration showed uniformity of thickness and carrier concentration of better than $\pm 0.1\%$ over the growth surface of a 2 inch diameter surface.⁹³

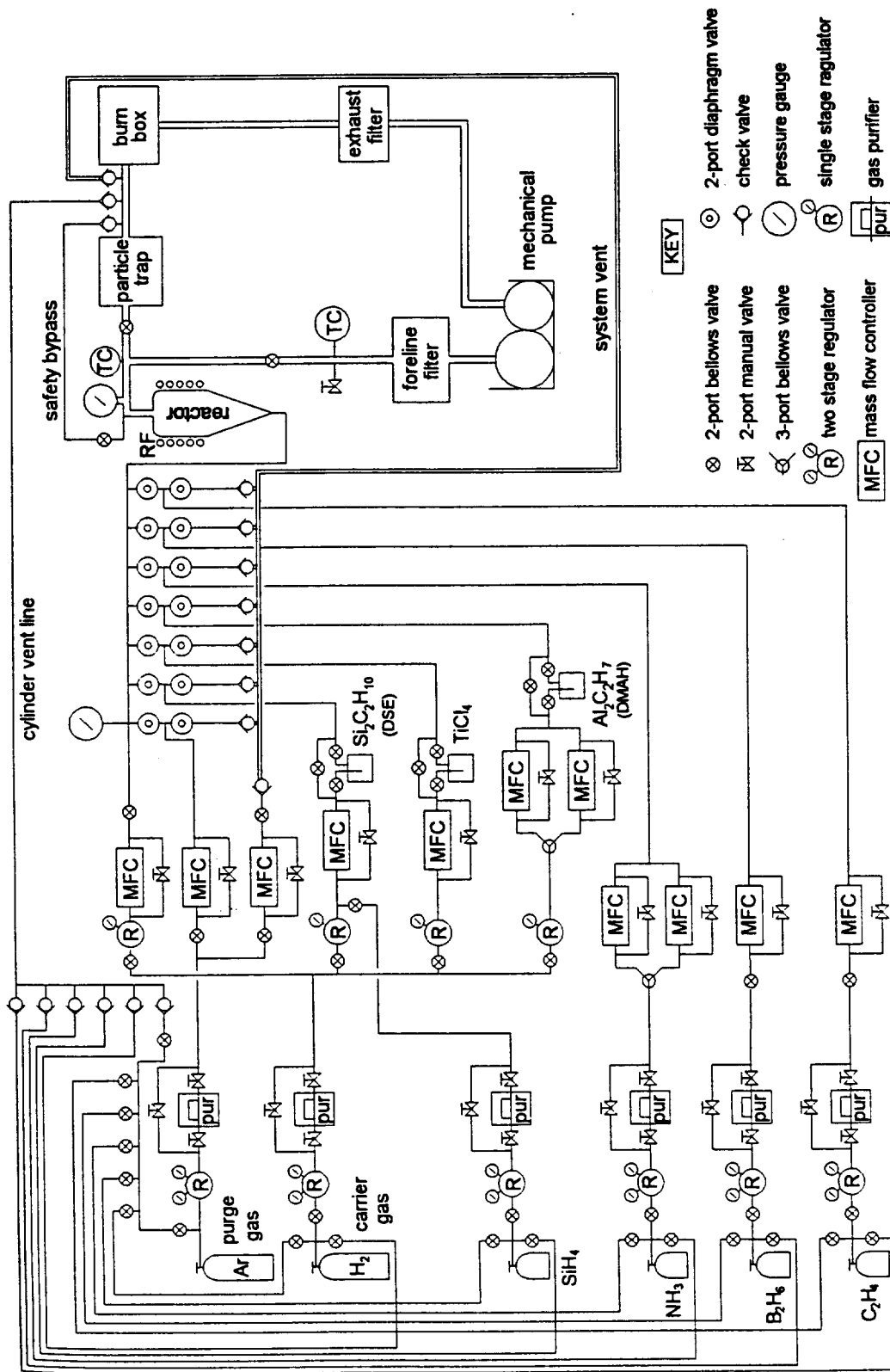


Fig. 3.1. Schematic diagram of β -SiC MOCVD system.

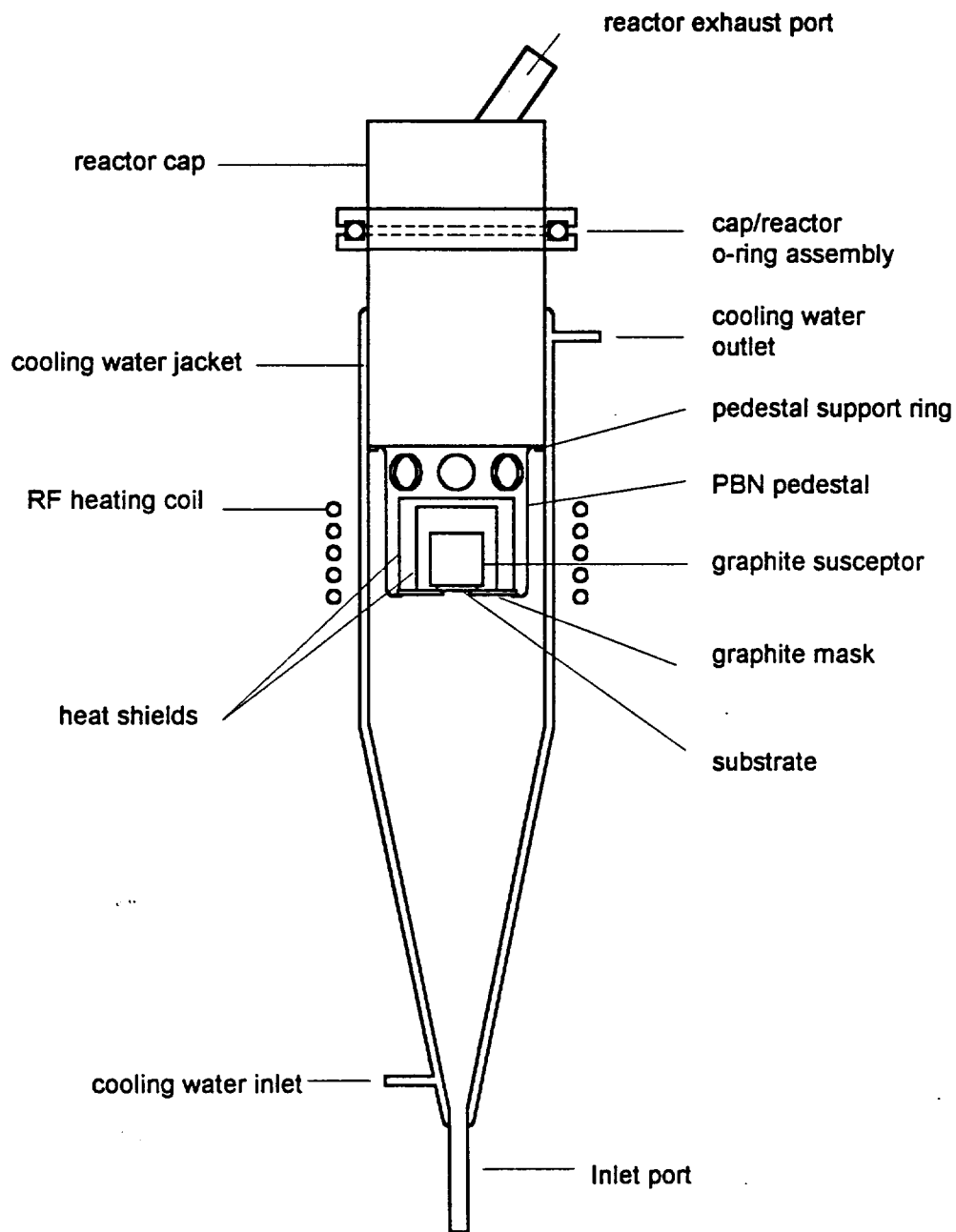


Fig. 3.2. Cross-sectional view of inverted-vertical CVD reactor.

3.2. β -SiC THIN FILM SYNTHESIS

β -SiC thin films were synthesized on TiC substrates using a single reactant source 1,2-disilylethane (DSE or $\text{Si}_2\text{C}_2\text{H}_{10}$) The choice of TiC substrate is discussed in the following section. The single reactant source has a single point of origin of C and Si atoms. Thus it offers a potential advantage of a more controllable growth process because there are fewer parameters, namely flow of C and Si reactant species, to control.

3.2.1. TITANIUM CARBIDE SUBSTRATE FOR β -SiC EPITAXIAL GROWTH

Substrate choice is a critical issue for epitaxial growth. The term epitaxy refers to the arrangement of atoms or molecules, in a unique orientation, upon a substrate which can be identical or different from the growing layer. In an epitaxial process the building of the crystal lattice occurs through the influence of the substrate atomic and molecular forces. Therefore the substrate has to possess physical and chemical properties favorable for single crystal epitaxial growth. These are: (1) crystal structure should be same, (2) lattice parameter mismatch should be minimal, (3) thermal expansion coefficient mismatch should be minimal, (4) the substrate should be chemically and thermally stable in the environment in which the growth process is occurring.

β -SiC grown on Si has high defect density because of large lattice mismatch between Si and β -SiC (~ 30%). $6H\alpha$ -SiC has a hexagonal crystal structure whereas β -SiC has a cubic crystal structure. This results in formation of double position boundary defects in β -SiC thin films grown on $6H\alpha$ -SiC. The

substrate best suited for single crystal β -SiC epitaxial growth has been determined to be titanium carbide.¹³⁸

The lattice parameter of titanium carbide is close to that of β -SiC (see table 3.2.). At room temperature the lattice mismatch between titanium carbide and β -SiC is less than 0.7%. Titanium carbide has same crystal structure as β -SiC, which is cubic (rock salt). This offers flexibility of growth orientation and reduces interface defect density. The melting temperature of titanium carbide (3150 °C) exceeds the sublimation temperature of β -SiC (~ 1800 °C). The growth temperature of β -SiC is below 1500 °C. The thermal expansion coefficient (α_t) of titanium carbide is approximately one and a half times the expansion coefficient of β -SiC. This causes lattice parameter mismatch at the growth temperature and thermal stress at the growth interface. However the fact that α_t (titanium carbide) is larger than α_t (β -SiC) causes the epilayer to be under compression instead of tension. A epilayer under tension is more likely to crack. Titanium carbide is stable at elevated temperatures in H₂ but reacts with oxygen at temperatures above 500 °C. Overall, the properties of titanium carbide are well within the limits of epitaxial single crystal growth requirements.

Table 3.2: Physical Properties of β -SiC and TiC.

Material	Lattice parameter (300 °K)	Crystal structure	Melting point	Thermal expansion coefficient (300 °K)
β -SiC	4.3596 Å	cubic (zincblende)	sublimes at > 1800 °C	$2.77 \times 10^{-6} \text{ K}^{-1}$
TiC	4.328 Å	cubic (rock salt)	3150 °C	$7.4 \times 10^{-6} \text{ K}^{-1}$

Table 3.2: Physical Properties of β -SiC and TiC.

Material	Lattice parameter (300 °K)	Crystal structure	Melting point	Thermal expansion coefficient (300 °K)
Reference	83,84	83,84	83,84	84,85

Titanium carbide also offers important advantages from point of view of β -SiC devices. It is a semimetal with a very low work function (~ 2.7 eV) and can form an ideal ohmic contact to β -SiC as well as $6H\alpha$ -SiC. The thermal conductivity of titanium carbide is higher than that of β -SiC below ~ 600 °C, which ensures effective heat dissipation from β -SiC device through the substrate in temperature regimes where the device is expected to operate.

3.2.2. TiC_x SUBSTRATE PREPARATION PROCEDURE

The standard titanium carbide substrate preparation procedure for β -SiC epitaxial growth consisted of 3 steps: (1) polishing, (2) de-greasing, (3) wet chemical etching.

The titanium carbide substrate was first lapped with a 15 μm diamond paste on a steel wheel. This was followed by 6 μm and 1 μm diamond paste polishing on a adhesive back nylon cloth until a specular surface was obtained. Then a chemical-mechanical polishing on a polishing pad was done for 3 minutes. This served the purpose of removing the mechanical damage caused by diamond polishing. The chemical-mechanical polishing solution developed by Parsons⁹⁵ has the following composition: 45 g of $\text{K}_3\text{Fe}(\text{CN})_6$, 1 g of KOH, 200 cm^3 of de-ionized water and 0.5 g of 0.05 μm Al_2O_3 powder.

The de-greasing was done in hot Tri-chloroethene, acetone and methanol for 5 minutes each. Then the substrate was rinsed with de-ionized water (DI water) and blow dried with nitrogen. Subsequently, two wet chemical etching procedures were performed on the substrate surface. The first was a 3 minute etch in 4.8% HF to remove any foreign oxides and the second was a 2 minute etch in $\text{HNO}_3:\text{H}_2\text{SO}_4::1:4$ acid mixture at room temperature to remove TiO_x on the surface and about 50 Å of titanium carbide layer. Finally the substrate was rinsed with DI water, blow dried in N_2 and immediately loaded into the CVD reactor.

3.2.3. GENERAL PROCEDURE FOR GROWTH

The β -SiC epitaxial growth was conducted in the inverted vertical reactor using the arrangement described in section 3.1. The temperature of the RF induction heated titanium carbide substrate was measured through the reactor chamber water cooling jacket with a Leeds and Northrup disappearing filament optical pyrometer. The angle of observation was about 20 degrees from the reactor chamber axis.

After loading the substrate, the system was pumped down to less than 1 millitorr and leak-checked, then back-filled with Ar. Then, a 3000 Å thick TiC buffer layer was grown on the titanium carbide substrate using the standard conditions described in section 4.3. After the TiC buffer growth, the substrate was heated to about 1600 °C for 10 minutes to remove chlorine reactant products from the previous growth, and then reduced to the temperature required for β -SiC. β -SiC growth was started by introducing the DSE ($\text{Si}_2\text{C}_2\text{H}_{10}$) carried by H_2 into the reactor. The DSE bubbler temperature was kept at 0 °C. The H_2 flow rate through the

bubbler varied from 2 to 6 sccm. The vapor flow rate of DSE was not determined because its vapor pressure has not been measured. Growth was terminated by bypassing the DSE source.

3.2.4. OPTIMIZATION OF GROWTH USING 1,2-DISILYLETHANE

This task was undertaken to achieve the following objectives: (1) controllable and repeatable growth, (2) single crystal, polytype free epilayers, (3) best possible growth morphology, (4) minimum possible growth temperature, and (5) maximum possible growth rate (for higher yield).

Temperature is very important for epitaxial single crystal CVD. It influences the growth in following ways:

(1) causes cracking of the reactant source

It should be high enough to ensure complete cracking of the source so that minor fluctuations in the temperature do not cause fluctuations in the cracking rate.

(2) causes the deposition reaction to proceed in the forward direction

(3) imparts surface mobility to the reactant species so that they can move to a lattice site favorable for single crystal epitaxial growth. Surface mobility increases with increase in the growth temperature.

(4) determines the sticking coefficient of the reactant species and impurities in the gas flow. The sticking coefficient decreases with increase in temperature.

(5) lower temperatures can reduce auto-doping from the reactor parts.

In case of β -SiC CVD using DSE source, the C/Si atomic ratio arriving at the growth surface depends on the cracking temperature. Also higher growth

temperatures cause larger lattice parameter mismatch because of difference in coefficient of thermal expansion of TiC and β -SiC. Therefore a low growth temperature is desirable but too low temperature can result in polycrystalline or poor quality layers.

TiC_x <111> substrates and a flow of 4 sccm H₂ gas through DSE bubbler was used in this study. The optimum temperature for nucleation was determined by Nomarsky and SEM observations of as-nucleated, polished and etched films grown at different temperatures. At $T_s < 1230$ °C, the films were polycrystalline and Si rich; the surface morphologies of these films were rough and impossible to polish to a smooth surface. At T_s greater than 1250 °C, the films were epitaxial, but they did not completely cover the substrate surface; the fraction of the TiC surface upon which β -SiC nucleation and growth occurred decreased with increasing temperature T_s . Optimum conditions for β -SiC nucleation were found to occur in a narrow range around 1240 °C.

The optimum growth temperature was determined by Nomarsky and SEM observation of surface morphologies of films nucleated at optimum nucleation temperature (1240 °C) and then grown at T_s from 1230 °C to 1400 °C. Growth at higher T_s was performed by first nucleating at 1240 °C and then ramping T_s to desired growth temperature. The criterion for optimum was the condition which gave specular as-grown morphology for the longest growth time. The best control of growth morphology was obtained by performing nucleation and growth at the same temperature value of 1240 °C. Fig. 3.4 shows the optimized thermal cycle for growth.

The effect of CVD growth conditions on the crystalline quality of β -SiC epilayers obtained from DSE is clearly shown in Fig. 3.5. The β -SiC epilayer grown by optimized conditions shows a smooth surface, without evidence of stacking faults, unlike the layer grown under non-optimized conditions. The optimum condition layer looked shiny with slight milkiess, to the naked eye. Determined by dektak measurements the surface roughness was of the order of 1000 Å.

The growth rate was measured from SEM cross-sections such as one shown in Fig. 3.6. The epilayer was grown with a flow rate of 4 sccm of H₂ through the DSE bubbler. The growth rate measured is about 5 $\mu\text{m}/\text{hour}$. Higher flow rates of carrier gas H₂ through the DSE bubbler to achieve higher growth rate, at the optimum temperature determined, resulted in polycrystalline layers. Electron channeling contrast pattern (ECCP) was used to determine whether the grown layers were single crystal or not. A ECC pattern can only be obtained from single crystal layers. Fig. 3.7 shows a ECC pattern obtained from a $\langle 111 \rangle$ oriented β -SiC epilayer grown at 1240 °C with a growth rate of 5 $\mu\text{m}/\text{hour}$.

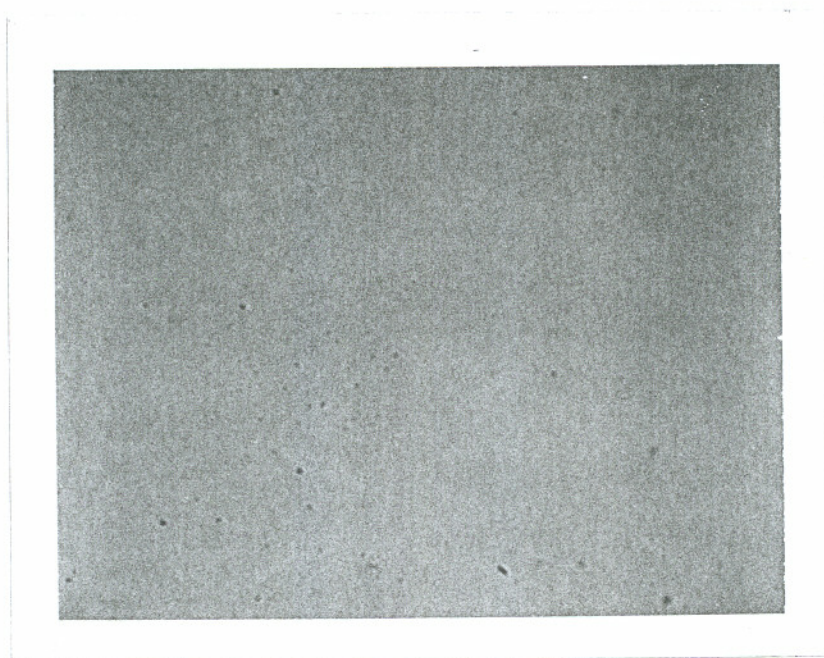


Fig. 3.3. Nomarsky photographs (30X) of a polished TiC substrate

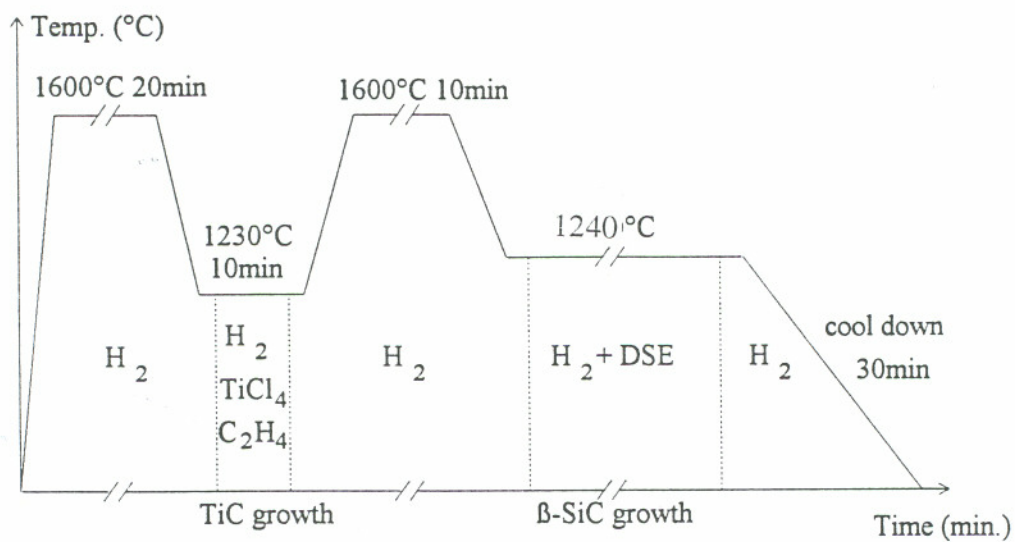


Fig. 3.4. Optimized thermal cycle for β -SiC growth on titanium carbide substrate.

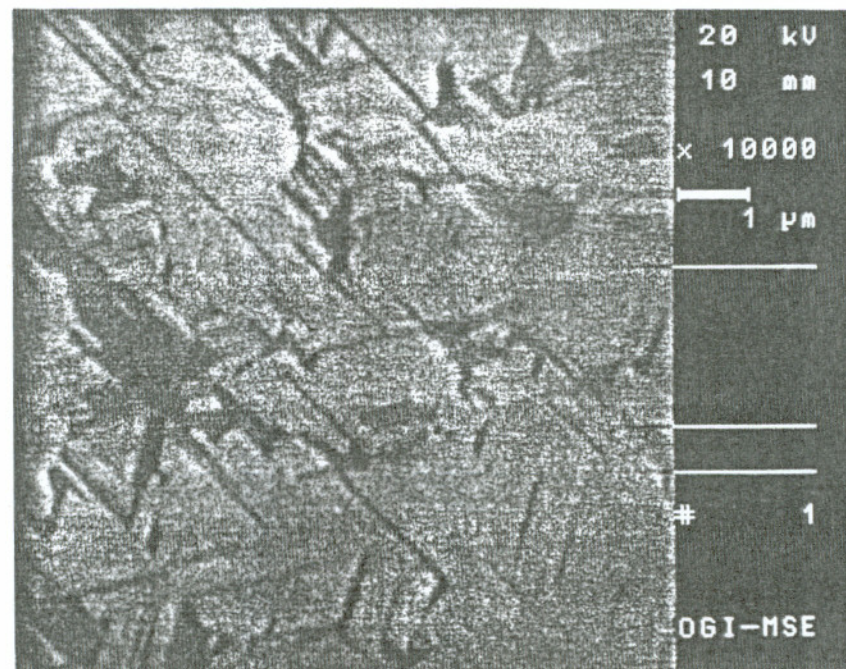
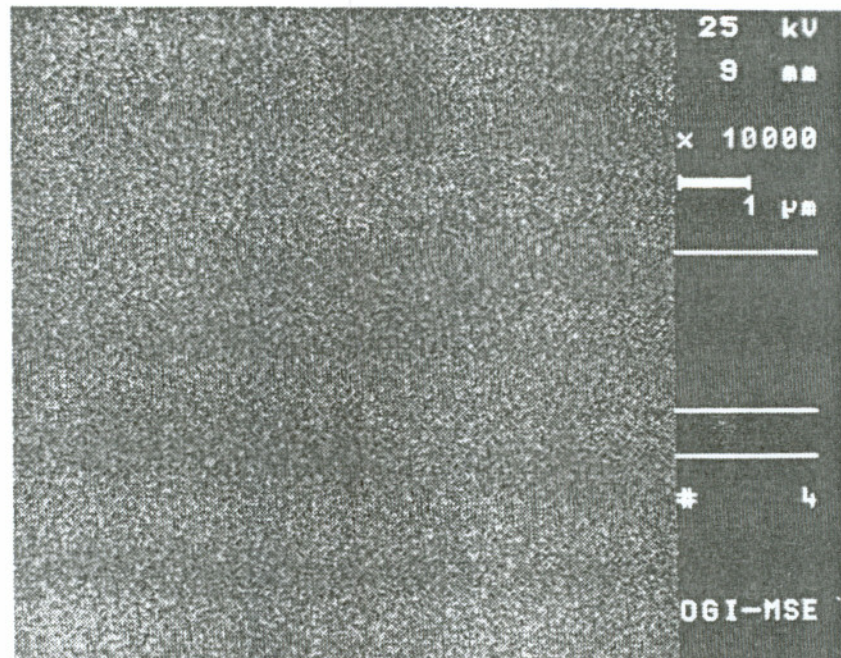


Fig. 3.5. S.E.M micrographs of polished β -SiC grown under optimized conditions (a) and unoptimized conditions (b).

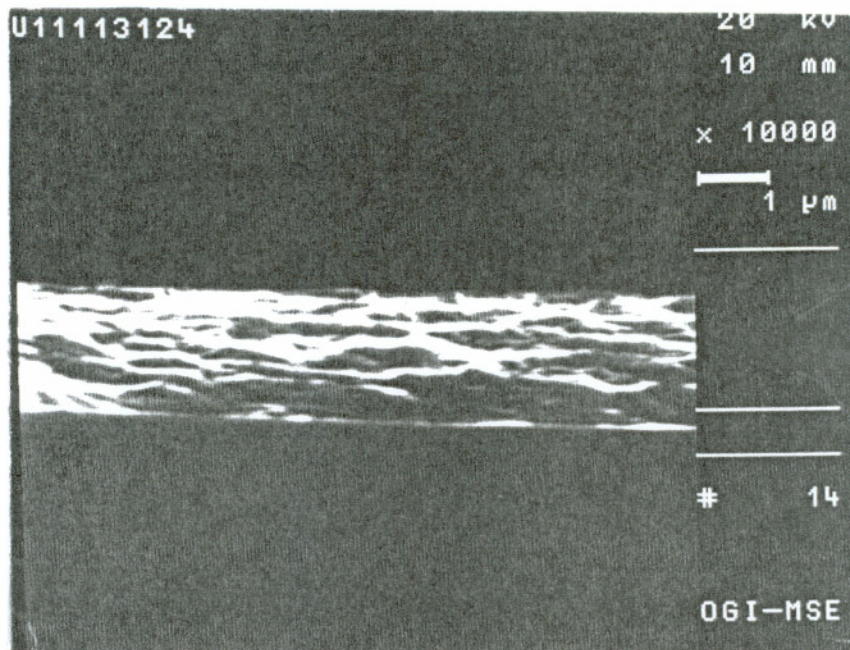


Fig. 3.6. SEM cross section of β -SiC/TiC interface for growth rate determination.

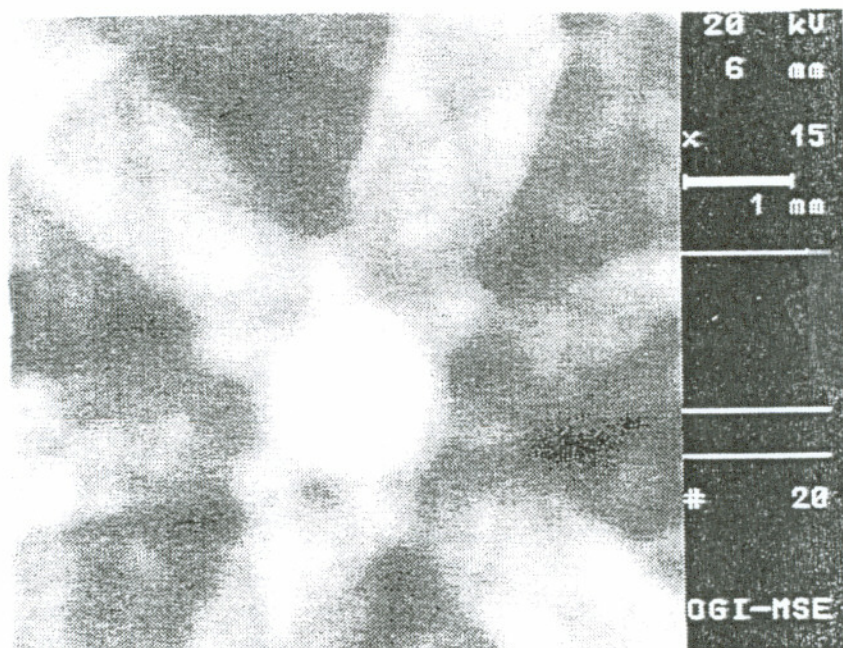


Fig. 3.7. Electron channeling contrast pattern from (111) β -SiC epilayer.

3.1. 6H α -SiC THIN FILM SYNTHESIS

Commercially available, bulk grown single crystal 6H α -SiC was used as substrate for 6H α -SiC thin film growth.¹² This is a homo-epitaxial growth process, and therefore more probable and easily controllable. The growth conditions used for epitaxial β -SiC on TiC substrate yield epitaxial single crystal 6H α -SiC when 6H α -SiC (0001) single crystal is used as substrate.

3.2. IN-SITU DOPING OF SiC EPILAYERS

Intentionally doped SiC was grown by introducing the desired dopant sources along with the 1,2-disilyl ethane source during the growth. Ammonia (NH₃), dimethylaluminum hydride (DMAH or Al₂C₂H₇) and diborane (B₂H₆) were used for *in-situ* doping to produce n-type, p-type and compensation isolation layers, respectively.

Optimized SiC growth conditions described in section 3.2.4 and 3.3 were used during *in-situ* doping. The flow rate of nitrogen used to degenerately dope the SiC epilayers for study of ohmic contacts was 0.0007 sccm for β -SiC sccm and 0.0013 sccm for 6H α -SiC. The flow rates used were based on studies done on incorporation of the dopant in SiC using SIMS technique by Parsons et al. at HRL.⁸⁷ Measurement of electrically active carriers, in case of high doping, in β -SiC was not possible because of high leakage currents in the Schottky diodes. The flow rate of boron was 0.27 sccm for growing β -SiC isolation epilayers and 0.29 sccm for 6H α -SiC isolation epilayers (see section 6.1.1 for isolation results).

3.3. SUMMARY

An inverted-vertical reactor MOCVD system was designed and constructed. A CVD epitaxial growth process for β -SiC, using TiC as a substrate and 1,2-disilylethane as reactant source, was developed and optimized. TiC was chosen as a substrate for β -SiC growth because of its comparatively much better lattice matching qualities. Optimum substrate temperature for β -SiC nucleation and growth was found to occur in a narrow range around 1240 °C. 1,2-disilylethane was also used for homo-epitaxial growth of 6H α -SiC thin films on 6H α -SiC substrate.

Boron doping was used for creating insulating layers and nitrogen doping for n-type layers.

CHAPTER 4

TiC AS A OHMIC CONTACT METAL & CONTACT FORMATION PROCESSES

This chapter describes the development of TiC ohmic contact metallization to n-type SiC. Following are the sections in this chapter; reasons for choosing TiC to form ohmic contact (section 4.1); reasons for selecting the two methods for ohmic contact formation, namely, MOCVD and sputter deposition (section 4.2); description of the developed contact formation processes (section 4.3); summary (section 4.4).

4.1. SELECTION OF OHMIC CONTACT METAL

As discussed in section 2.4, metals selected to form ohmic contacts to SiC are prone to formation of carbides/silicides at the metal/semiconductor interface due to high temperature operation of SiC devices. This led Parsons et al.^{87,93,94} to investigate direct deposition of carbide or silicide, instead of using elemental metals. Extensive experiments were performed on ohmic contact formation, adhesion and stability. The results of these studies confirmed that stoichiometric TiC is the preferred contact metal for ohmic contacts to n-type SiC.

Stoichiometric titanium carbide, TiC, is semi-metal with a low work

function compared to that of n-type SiC. The work function of TiC is about 2.7 eV and of n-type SiC greater than 4.0 eV (because the electron affinity is about 4.0 eV^{27,88}). The exact value for the semiconductor work function depends on the doping level because it is the difference between the vacuum level and the Fermi level. When the work function of the metal is less than that of an n-type semiconductor, as is the case for TiC/n-type SiC, they will form an ideal ohmic contact if the interface state density (Tamm states^{89,90}) is below about 10^{12} per square-cm.⁹¹ An ideal ohmic contact is the one where the work function difference between the metal and semiconductor control the Schottky barrier height. The interface state density can be reduced to a value many orders of magnitude below 10^{12} cm² by reducing the number of dangling or unsatisfied bonds, when the interface is epitaxial.⁹³ This ideal situation is achieved in case of lattice matched single crystal TiC/n-type β -SiC and 6H α -SiC epitaxial interfaces.

TiC is also a low resistivity semi-metal. The resistivity of TiC_x decreases as x increases.^{85,86} The minimum resistivity of stoichiometric TiC is projected to be about 70 μ ohm-cm. However, reference no. 86 reports a resistivity of 100 μ ohm-cm for TiC_{0.95} which is much lower than that reported in ref. 87, and indicates that the resistivity of stoichiometric TiC may be less than 10 μ ohm-cm. This is competitive with or superior to the resistivity values of ohmic contact metals now in use.

The melting temperature of TiC is about 3150 °C, and it does not decompose or undergo phase transformations in any temperature range of interest for SiC epitaxial growth, or for SiC device applications at high temperature.

The prediction of stability of TiC/SiC interface at high temperature and high

power operating conditions was based on:⁸⁷ (1) Gibbs free energy of formation curves (Ellingham diagrams) of carbides and silicides and (2) measurement of electrical characteristics and Auger electron spectroscopy (AES) of Ti/SiC contacts after annealing at high temperatures. The results obtained show that Ti prefers to form a carbide and the formation of silicide is unlikely in the presence of free carbon.

These above mentioned characteristics made TiC an ideal choice for ohmic contact metallization to SiC.

4.2. CHOICE OF METHODS FOR OHMIC CONTACT DEPOSITION

TiC was chosen to be deposited by DC sputtering and MOCVD. Chemical vapor deposition was used to obtain an epitaxial single crystal TiC/SiC interface. Such an interface was expected to provide minimum attainable specific ohmic contact resistance, as discussed in section 4.1.

DC sputtering has the advantage of being a low temperature process (desirable for easier integration into IC processing) and the disadvantage of yielding polycrystalline TiC layers. DC sputtering was selected over e-beam evaporation because of the high melting temperature of TiC. The specific ohmic contact resistance was measured after annealing the sputtered contacts.

4.3. EPITAXIAL TiC DEPOSITION BY MOCVD

The technique for titanium carbide thin film synthesis by MOCVD was developed¹³⁷ to serve a two fold purpose: (1) as one of the methods for ohmic

contact metallization to n-SiC and (2) to obtain more stoichiometric, relatively lower defect density, epitaxial TiC on the substrate. The epitaxial TiC serves as a buffer layer, i.e., provides a new, better quality surface for subsequent nucleation and growth of β -SiC.

The growth sources used for TiC growth are TiCl_4 and C_2H_4 . H_2 is the carrier gas. The substrate was heated to T_s ($T_s = 1230\text{ }^\circ\text{C}$ for growth on titanium carbide and $1260\text{ }^\circ\text{C}$ for growth on SiC) in 2.9 standard liter per minute H_2 and stabilized for TiC growth. Next, 0.54 sccm of C_2H_4 was introduced into the reactor and thirty seconds later, 0.85 sccm of TiCl_4 vapor carried by 100 sccm H_2 was introduced to start the TiC growth. C/Ti was about 1.3. The growth rate of the TiC thin film was $1.7\text{ }\mu\text{m/hr}$.

The surface morphology of the as grown TiC layers was investigated by scanning electron microscope. Fig. 4.1 shows the surface morphology of a TiC film grown on (0001) $6\text{H}\alpha$ -SiC substrate. Under the Nomarsky microscope a defect free smooth surface was observed.

Electron channeling contrast pattern (ECCP) was used to determine single crystallinity of the grown layers. A single crystal film gives an electron channeling pattern, as shown in the Fig. 4.2, obtained from a 3000 \AA thick TiC layer grown on a (0001) $6\text{H}\alpha$ -SiC substrate. The penetration depth of channeling electrons is about 500 \AA , therefore this technique is well suited for thin film single crystallinity characterization.

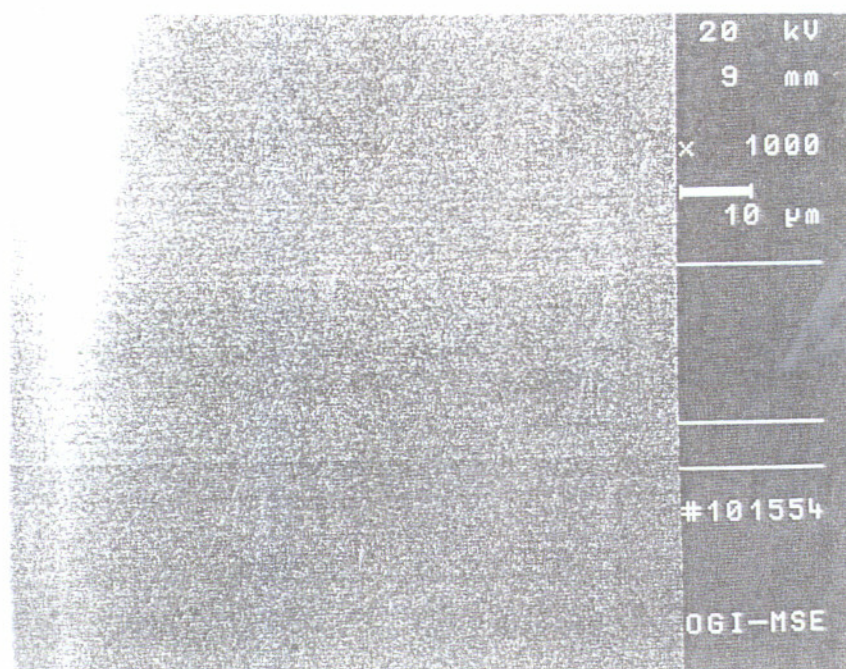


Fig. 4.1. SEM micrograph of a TiC epilayer grown on 6H α -SiC.

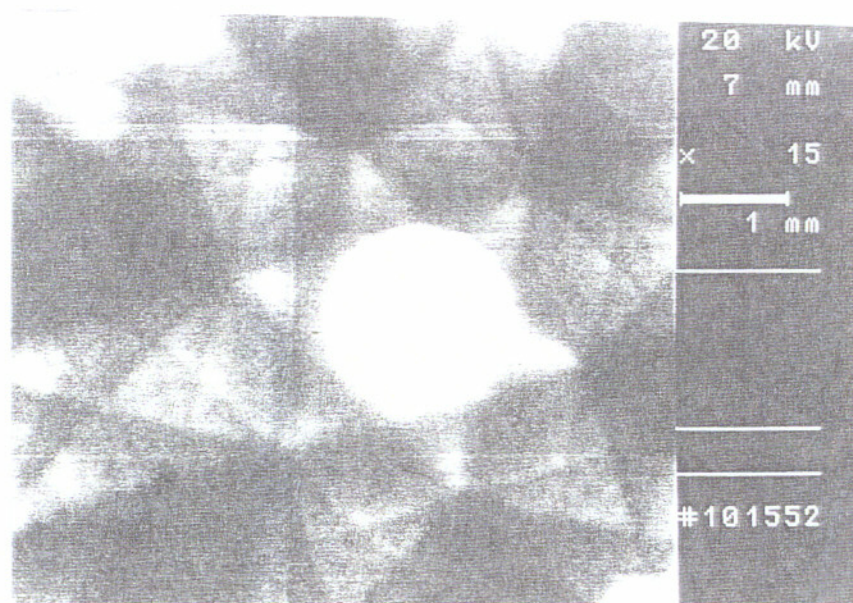


Fig. 4.2. Electron channeling contrast pattern from a TiC epilayer grown on (0001) 6H α -SiC.

4.4. POLYCRYSTALLINE TiC DEPOSITION

Polycrystalline TiC ohmic contacts were formed by sputter deposition. This section gives: (1) an overview of the sputter deposition method together with discussion of the factors / parameters involved in development of TiC sputter deposition process, (2) description of the sputter deposition apparatus and the developed experimental procedure including obtained TiC deposition characteristics.

4.4.1. SPUTTER DEPOSITION METHOD

Sputtering¹¹⁴ is a physical deposition process used widely in IC processing for deposition of both metals and insulators. It has the ability to deposit alloys with the composition similar to that of the target. Coverage of sputter deposited films is same as that of electron beam evaporated, but they show better adhesion and high density because of the characteristic high impact energy of the sputtered material on the substrate. TiC for ohmic contact study was sputter deposited because of above-mentioned advantages and the fact that high melting temperature of TiC disallows the use of e-beam evaporation.

Sputtering involves the acceleration of ions, usually Ar^+ , through a potential gradient, and the bombardment of these ions on a target or the cathode. Through momentum transfer, atoms near the surface of the target material are dislodged or sputtered and they impact the substrates with relatively high kinetic energies (can be up to several electron volts). The process is accomplished in an evacuated chamber and the pressures range from few millitorr to about 100 millitorr. Either dc or rf

glow discharge, in a diode system, can be used.

Often, the ion current density to the electrode (target) is increased by the aid of magnetic fields¹¹⁵⁻¹¹⁷ which capture the electrons and cause higher ionization in the discharge than would normally occur. This results in higher sputtering rates and also facilitates sputtering of materials which form tenacious oxides like Al and Ti. Such sources are called magnetron sources.

The most fundamental parameter of sputtering processes is the sputtering yield. It is defined as the number of atoms ejected from a target surface per incident ion and is related to the momentum transfer from energetic particles to target surface atoms. There is a threshold for sputtering that is approximately equal to the heat of sublimation. In the energy range of practical interest for sputtering processes (10-5000 eV), the yield increases with incident energy, and with the mass and d-shell filling of the incident ion.^{118,119} The sputtering yield determines largely, but not completely the deposition rate of the sputtered films. This is because in glow discharge systems, bombarding ions are by no means mono-energetic, and it is not necessarily valid to use yield values for pure metals when alloys, compounds or mixtures are sputtered. Therefore yield values are used to give a rough indication of expected etch or deposition rate.

For a given target material both deposition rate and uniformity are influenced by system geometry, target voltage, sputtering gas, gas pressure, and power.¹²⁰ All other things being equal, rates are linearly proportional to power and decrease with increasing target-substrate separation. The sputtering gas influences the deposition rate the same way it influences sputtering yield.

As the gas pressure is increased the discharge current increases (increasing deposition rate), but return of the material to the target by backscattering^{121,129,131} also increases (decreasing deposition rate). Backscattering occurs due to simple collisions of the sputtered material in the gas phase. Along with the above mentioned two competing processes, another process termed Penning ionization,¹²² increases at higher pressures which increases the rate by self-sputtering. Excited metastable neutrals of the sputtering gas are formed by collisions of electrons with ground-state gas atoms. The sputtered neutral atoms can be ionized by the Penning mechanism (the collision of a metastable neutral with a ground-state neutral to produce an ion and return the metastable neutral to the ground state) when the first ionization potential of the sputtered atom is less than that of the metastable energy. Since the metastable energies of the noble gases are greater than the first ionization potential of most elements, this mechanism can produce a copious supply of ions which can bombard substrates surfaces and/or return to the target to cause self sputtering.¹²³ Thus the amount of Penning ionization that occurs depends on the nature of gas and increases with increasing gas pressure. The sum of all this leads to a gas pressure or a small range of gas pressures at which the rate is maximum, which must be determined empirically. Another effect of increasing sputtering gas pressure is to slow energetic particles by inelastic collisions. This effect can be used to maximize or minimize the energy of particles incident on the substrates.

The flux of sputtered material to the receiving substrate is dependent on the cosine of the angle, ϕ , between the normal to the source surface and the direction of the receiving surface a distance r away. If θ is an angle between the receiving

surface normal and the direction back to the source, then

$$D = \frac{R}{\pi r^2} \cos \phi \cos \theta \quad (4.1)$$

where D is the deposition rate and the R is the total loss of the material from the source per unit time and depends on sputtering conditions. When the receiving surface is spherical and has a radius r_0 , and the source is on the surface (see Fig. 4.3), then

$$\cos \theta = \cos \phi = \frac{r}{2r_0} \quad (4.2)$$

and Eq. 4.1 is written as¹²⁴

$$D = \frac{R}{4\pi r_0^2} \quad (4.3)$$

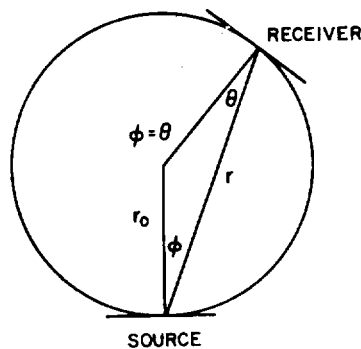


Fig. 4.3. Idealized view of a source and a substrate mounted on a sphere.

Therefore, the deposition rate is the same for all points on the spherical surface, which is the principal behind the planetary substrate supporting system used in deposition chambers. This implies that for large substrates, uniformity of

deposition across the surface will improve with larger distance from source because as the radius of curvature of the sphere on which the substrate rests becomes larger, the substrate surface can be better approximated to be part of the sphere. Since the deposition rate is inversely proportional to square of the distance from the source, a optimum separation distance is sought. For smaller substrates the optimum separation distance is smaller. The edges of the target no matter how the dark space shield is constructed, represent regions of gross non-uniformity leading to a finite minimum achievable non-uniformity.

Pressure gradients in the vicinity of the sputtering targets produce nonuniform bombardment and film deposition. Local pressure gradients can occur at the target surface (because of gettering), near the pumping port, or at points of high or low temperature relative to rest of the system. To offset this problems it is often necessary to introduce gas at more than one point in the system. This is especially a problem in very large systems.

Usage of high gas flow rates enables constant sweeping out of impurities in the sputtering chamber.¹²⁵ This implies that the pumping system used must be operated to obtain maximum pumping speed for the gases used.

In addition to neutral particles, there are secondary electrons and ions, reflected incident particles, which are produced at the target and are a source of bombardment of the growing film. Desorption of gases, especially from hot-pressed targets¹²⁶ and powder targets¹²⁷, can contaminate or effect the deposition rate of the film. The highest purity work is done with very dense targets e.g., vacuum cast or arc-melted materials. UV and visible light photons, x-rays emitted from the target

can cause radiation damage of surface sensitive substrates.

4.4.2. SPUTTER DEPOSITION APPARATUS & EXPERIMENTAL PROCEDURE

The sputtering system used for this study has a 5-inch, 7.5 kW Varian S-gun magnetron source in which 99.99% purity TiC target (cathode) is mounted. Magnetron sources are low impedance (high current low voltage) sources which operate at relatively low pressures while conventional dc or rf diode sources are high impedance (high voltage low current) sources operating at higher pressures. To maximize film deposition rates in conventional sputtering diodes, the cathode is placed close to the substrates which are on the anode, and a maximum potential is applied to the cathode. However, bombardment of the substrates by the secondary electrons occurs causing heating and thermal degradation of the substrates. On the other hand magnetrons have high cathode erosion rates and yield useful deposition rates with substrates supported in planetary support systems. Thus there is a lot less heating of the substrates. The system used for this research work is set up to support only one substrate at a time.

S-gun magnetrons utilize circular cathodes and concentric central anodes as shown in Fig. 4.4. The cathode is clamped without bonding into a water cooled housing. The contact to cooled metal is achieved through thermal expansion of the cathode during sputtering operation. The anodes are also water cooled and insulated, permitting them to be electrically biased. An annular permanent magnet assembly is used to obtain the magnetic field and values of 0.015 T are typical of the flux density

near the cathode.

Electrons emitted by the cathode are trapped by the influence of the magnetic field and are forced to travel in long helical paths. As they travel along the magnetic field lines, the electrons make elastic or ionizing collisions with the argon gas atoms. The magnetic field makes it possible to generate a current density orders of magnitude greater than in dc or rf planar diode sputtering systems.

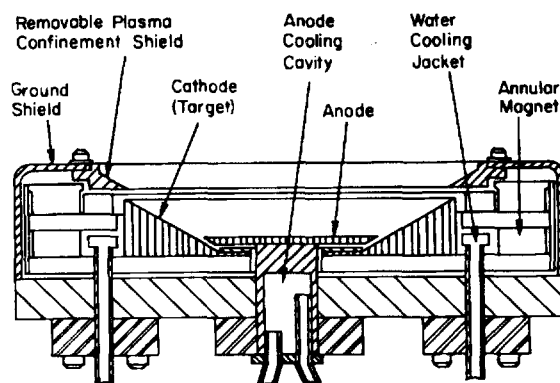


Fig. 4.4. Cross-section view of the 5 inch S-gun (courtesy Varian assoc.).

A cryo pump aided by a sorption pump was used to create vacuum. Diffusion pump and mechanical pump were not used because these can cause contamination due to back-streaming of oil from the pumps into the sputtering system. The cryopump and the sorption pump work on the principles of cryocondensation and cryosorption.

Cryosorption is the ability of a cold substance to cool a gas, thereby reducing its pressure, and prevent its returning to the chamber. This is accomplished in a cryosorption pump, by using a liquid nitrogen cooled ($-196\text{ }^{\circ}\text{C}$) and highly porous molecular sieve material (zeolite). The high porosity gives the zeolite a tremendous

surface area. The gas molecule gets trapped in the molecular sieve, bounces around and progressively loses its thermal energy and is thus finally caught. Though primarily cryosorption, some cryocondensation occurs in the sorption pump too. It is capable of rough pumping down to 10^{-3} torr.

The sticking of most molecules to a chilled surface of around 20° K is called cryocondensation. At this temperature, the combined partial pressures of most gases is around 10^{-9} torr. Cryocondensation alone is not sufficient to obtain the necessary vacuum. Gas molecules like neon, helium and hydrogen do not stick to a chilled surface due to their high vapor pressures. Such molecules have to be removed by cryosorption. Cryocondensation and cryosorption both take place in a cryopump which utilizes pure helium as a coolant to cool the expansion unit, which is also called 'cold head'. The 'cold head' is shaped like an inverted bucket. The inner surface of this is coated with activated charcoal to capture molecules by cryosorption while the outer surface is uncoated, and cryocondensation occurs on it. A compressor is used to compress helium from 100 psi to about 300 psi. An oil separator is used to filter out any oil from the helium after it passes through the oil lubricated compressor, otherwise the oil would solidify and destroy the expansion unit.

The SiC substrate was de-greased in hot tri-chloroethene, acetone and methanol for 5 minutes each. Then it was rinsed with de-ionized water (DI water) and blow dried with nitrogen. A 3 minute etch in 4.8% HF was performed to remove any foreign oxides. Finally the substrate was rinsed with DI water, blow dried in N_2 , mounted on a sputtering substrate holder and loaded into the sputtering system.

The chamber was first evacuated to a pressure of about 2×10^{-6} torr, then backfilled with argon to the desired operating pressure. During operation, the chamber was constantly pumped through two bellows sealed valves, whose opening was manually adjusted to maintain the pressure at the desired level. Ar flow rate to the chamber was controlled by using a standard mass flow controller. After the operating pressure had stabilized the dc power supply was turned on.

Pre-sputtering of TiC targets was done to clean and equilibrate target surface prior to film deposition with the shutter, situated over the target, closed. This helped remove any surface oxides, brought the target surface to thermal equilibrium, and outgassed the system. Initially, oxides with high secondary electron emission ratio are sputtered and background gaseous contaminants are broken down (especially H_2O), leading to high discharge current which gradually decreased as the contaminants were removed from the system and/or covered up with sputtered material. The pre-sputtering was terminated when the discharge current fell to a constant value.¹³¹

Next, sputter etching of the substrate was done. A modification was made in the system such that an electrode could be swung into position about 3 cm below the substrate. Then a 500 V ac voltage was applied to this electrode to sputter etch the substrate. The substrate was grounded. Sputter etching was done for 5 minutes.

De-greasing of the substrate prior to loading was necessary because any organic contaminant on the surface can get polymerized due to inert ion bombardment during sputter etching and become very difficult to remove.^{128,129} Organic contamination can also occur due to backstreaming vacuum pump fluids

and usage of cryo and sorption pump prevented it. With glow discharge sputter etching, it is rarely possible to obtain an atomically clean surface. In general, this is only possible in a ultra high vacuum system using ion beams followed by high temperature annealing.¹³⁰ One reason very clean surfaces are difficult to obtain is backscattering. The return of the sputtered material, which may not only be the material sputtered from the substrate but also from surroundings like the substrate holder, can form a new composite surface. This was minimized by using a high target voltage and low operating pressure. Very high target voltages are not used because they increase crystallographic damage of the surface. Use of radio-frequency for target excitation with sputter-etch voltages around 2 kV or more has been reported to decrease backscattering in literature¹³¹ Reactive gases similar to those used for plasma etching, reactive ion etching e.t.c. also have shown to produce exceptionally clean etched surfaces.¹³²

Fig. 4.5 and Fig. 4.6 show the TiC sputter deposition rates obtained as a function of applied power at constant pressure and as a function of ambient pressure at constant power, respectively. These curves are in accordance with the sputter deposition rate dependance mentioned in section 4.4.1 and also show existence of a optimum gas pressure. TiC ohmic contacts for the study were sputter deposited at 2000 W and 15 millitorr Ar gas pressure. The substrate was connected to ground. The separation distance between the S-gun magnetron source and substrate, directly above the source, was 30 cm. The flow rate of Ar was 40 sccm. The deposition rate measured from cross-sections by S.E.M., was 500 Å/min.

The sputtered TiC films were formed and annealed in H₂ (section 5.1.2).

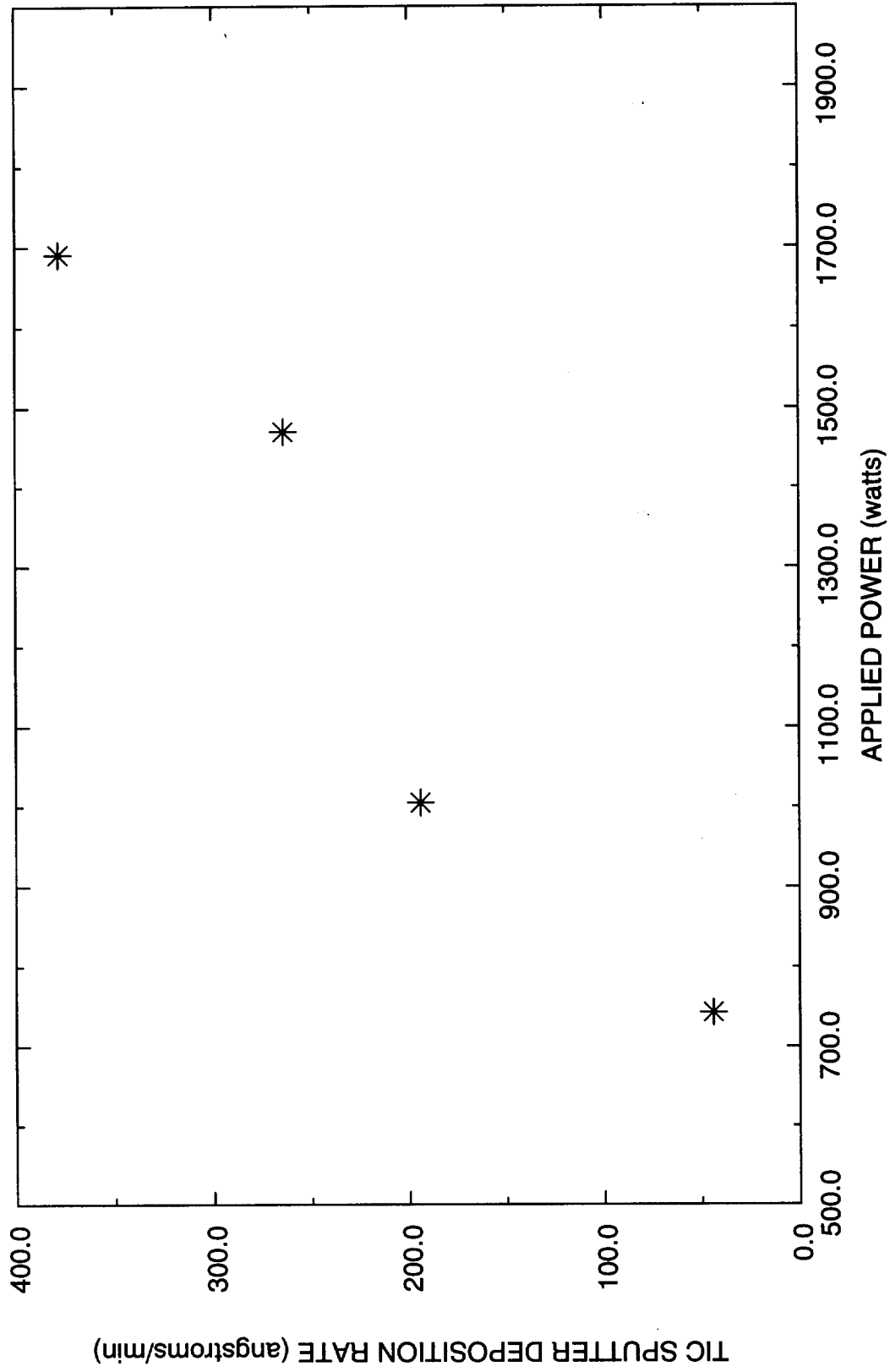


Fig. 4.5. TiC sputter deposition rate versus power at constant gas pressure of 15 ± 1 millitorr.

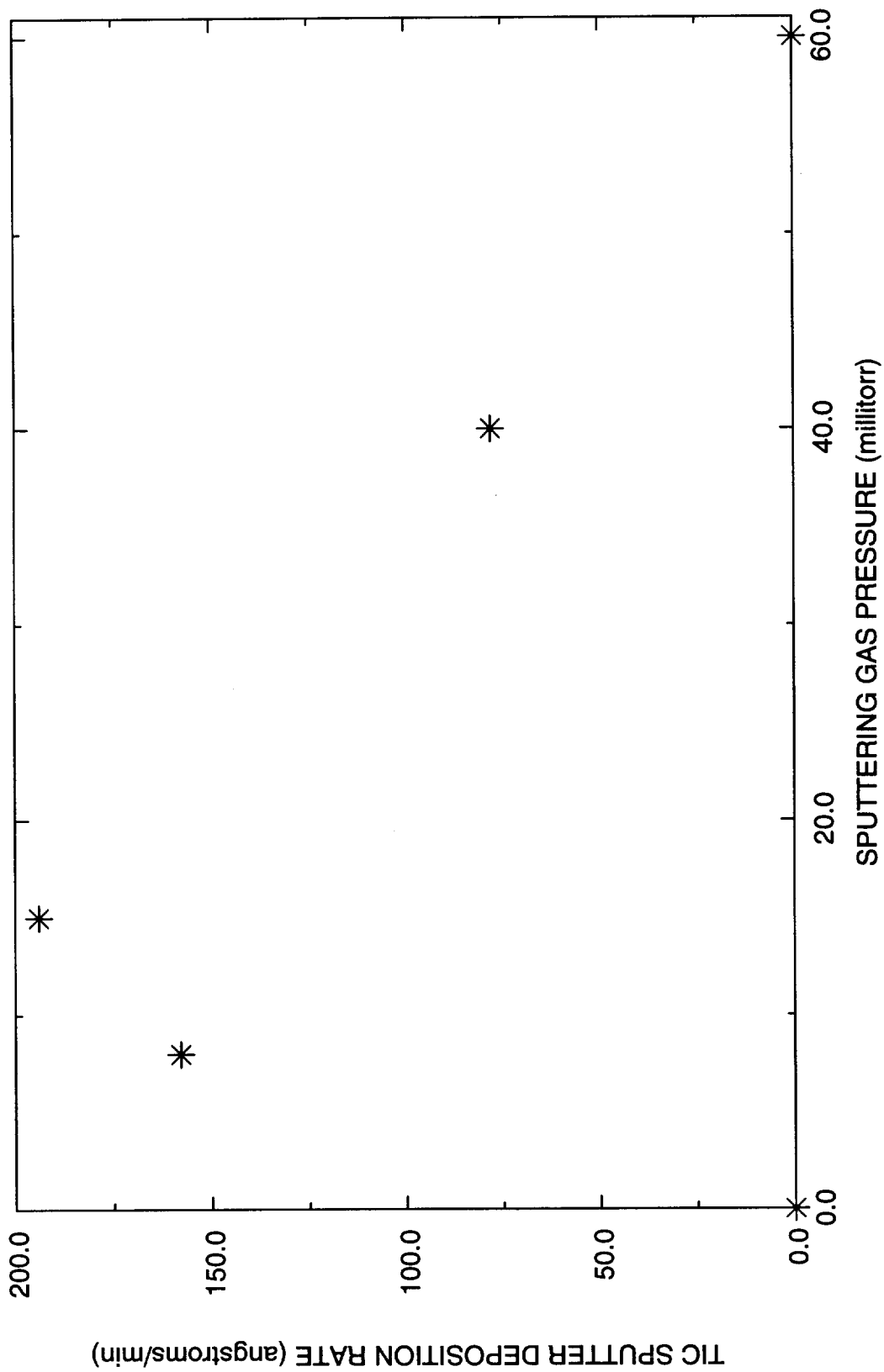


Fig. 4.6. TiC sputter deposition rate versus sputtering gas pressure at constant power of 1000 ± 15 W.

4.5. SUMMARY

The low work function, low resistivity, high predicted stability of TiC and TiC/SiC interface and ability to form epitaxial interface with SiC made TiC an excellent choice for ohmic contact metallization to n-type SiC. MOCVD and sputter deposition methods were used to form TiC ohmic contacts. TiCl_4 and C_2H_4 were used as reactant sources for epitaxial growth of TiC thin films by MOCVD, on SiC epilayers at $T_s = 1260$ °C. TiC was dc sputter deposited using S-gun magnetron source. TiC sputter deposition rate varied linearly with power at constant pressure and showed a maxima when plotted as a function of gas pressure at constant power. A sputter deposition rate of 800 Å/min at 7 millitorr gas pressure and 1820 W was used for TiC metallization.

CHAPTER 5

CHARACTERIZATION METHODS & PROCEDURES FOR TiC OHMIC CONTACTS

This chapter presents the characterization methods and procedures used to assess the properties of TiC ohmic contact metallization to n-type SiC. The characterization was achieved by using three methods: (1) measurement of the specific ohmic contact resistance (section 5.1), (2) determination of stability of TiC/SiC interface (section 5.2), (3) determination of hardness and adhesion of TiC contacts to SiC (section 5.3). Section 5.1 further consists of theoretical background of specific contact resistance measurement technique, description of process steps to fabricate the test structures for measuring the specific ohmic contact resistance and procedure used to perform the electrical measurements.

5.1. MEASUREMENT OF SPECIFIC OHMIC CONTACT RESISTANCE

The measurement of specific contact resistance,¹⁰⁵ at room temperature, of TiC ohmic contacts to n-type SiC was one of the methods used to evaluate them. The measurement was based on transfer length method¹⁰⁶ which is a commonly used method and is described in section 5.1. The sample was first processed into

transfer length measurement (TLM) structures by photolithography as described in section 5.1.2. After the processing, a probe station and HP4145B semiconductor parameter analyzer were used to measure the specific contact resistance (R_s).

5.1.1. THEORY OF MEASUREMENT TECHNIQUE

Specific interfacial contact resistance,^{28,107} for a metal semiconductor contact, is the reciprocal of the derivative of current density with respect to voltage, at zero bias:

$$\rho_i = \left(\frac{\partial J}{\partial V} \right)^{-1} \Big|_{V=0} \quad (5.1)$$

It is generally represented in ohm-cm² units. It is a theoretical quantity and is not actually measurable. The parameter that can be measured is contact resistance from which specific contact resistance is calculated. The inability to measure just the specific interfacial resistance arises because, the measured contact resistance not only includes the specific interfacial resistance but also a portion of the metal immediately above the metal-semiconductor interface, a part of the semiconductor below that interface, current crowding effects, spreading resistance under the contact, and any interfacial oxide that may be present between the metal and the semiconductor.

The doping should be as high as possible for lowest interfacial resistance.¹⁰⁸ Lowering of the interfacial resistance also lowers the specific contact resistance. The theoretical calculation of specific interfacial resistance for individual cases is not only complex but is of little practical value as it does not describe the behavior of

the real contact.

The measurement technique used in this study, known as transfer length method, was originally proposed by Shockley.¹⁰⁹ The test structure used for the measurement uses 6 identical TiC contacts with unequal spacing between them of 10 μm , 20 μm , 40 μm , 80 μm and 160 μm . The contacts were either DC sputtered or chemical vapor deposited on a degenerately n-doped SiC epilayer. Assuming identical contact resistances for all contacts allows the total resistance to be written as:

$$R_{Ti} = \rho_s \frac{d_i}{Z} + 2R_c \quad (5.2)$$

where $i = 1, 2, 3, 4, 5$ or 6 . R_c is the contact resistance, d is the spacing between contacts, Z is the width of the contact and ρ_s is the sheet resistance. For the configuration shown in Fig. 5.1., with the contact width Z equal to the width of the doped semiconductor sheet W , the contact resistance is given as:¹¹⁰

$$R_c = \frac{(\sqrt{\rho_s \rho_c})}{Z} \coth\left(\frac{L}{L_T}\right) = \frac{\rho_c}{L_T Z} \coth\left(\frac{L}{L_T}\right) \quad (5.3)$$

R_c is sometimes referred to as the contact front resistance. ρ_c is the specific contact resistance, L is the contact length and $L_T = \sqrt{\rho_c / \rho_s}$ is defined as the transfer length. It can be considered as the length where the voltage due to the current transferring from the semiconductor to the metal or from the metal to the semiconductor has dropped to $1/e$ of its maximum value. It is equal to the effective length of the contact which is actually used for passage of the current. In other words the effective contact length can be much smaller than the actual contact

length L . LZ is the actual contact area whereas $L_T Z$ is the effective contact area. The reduction of the contact length used has important consequences because it can increase the current density to a value high enough to cause burn out. Two cases lead to simplification of Eq. 5.3:

First, for $\frac{L}{L_T} \leq 0.5$,

$$R_c \approx \frac{\rho_c}{LZ} \quad (5.4)$$

and second for $\frac{L}{L_T} \geq 1.5$,

$$R_c = \frac{\rho_c}{L_T Z} \quad (5.5)$$

The effective contact area is the actual contact area in the first case, but in the second case it is contact width times the transfer length.

Equation 5.3 is derived under the assumption that $\rho_c > 0.2\rho_s t^2$, where t is the conductive semiconductor epilayer thickness. The transfer length method has to be modified if the above condition is not satisfied.¹¹¹

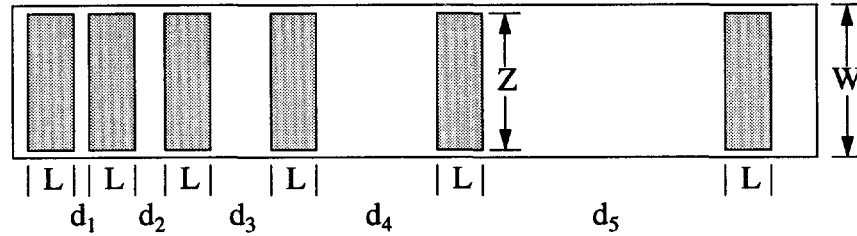
For contacts with $\frac{L}{L_T} \geq 1.5$, Eq. 5.2 can be written as:

$$R_T = \frac{\rho_s d}{Z} + 2R_c \approx \frac{\rho_s d}{Z} + 2\frac{\rho_s L_T}{Z} \quad (5.6)$$

where approximation given by Eq. 5.5 has been used. The total resistance is measured for various contact spacings d . R_T is plotted as a function of d as illustrated in Fig. 5.1. Three parameters can be extracted from such a plot. The slope $= \rho_s/Z$ leads to the sheet resistance, with the contact width Z independently measured. The intercept at $d = 0$ is $R_T = 2R_c$, giving the contact resistance. The

intercept at $R_T = 0$ gives $d = 2L_T$, which in turn can be used to calculate the specific contact resistance using ρ_s known from the slope of the plot and the relation $L_T = \sqrt{\rho_c / \rho_s}$.

The transfer length method gives a complete characterization of the contact by providing the sheet resistance, the contact resistance, and the specific contact resistance. The intercept at $R_T = 0$ giving L_T can sometimes be not very distinct leading to incorrect ρ_c values. The veracity of these values also depends on the fact that sheet resistance under the contacts is the same as the sheet resistance between contacts and is unchanged due to the process of contact formation. This method also neglects the resistance of the metal, which introduces little error if the metal resistance is low.



$L = 30 \mu\text{m}$, $W = 100 \mu\text{m}$, $Z = 10 \mu\text{m}$, $d_1 = 10 \mu\text{m}$, $d_2 = 20 \mu\text{m}$,
 $d_3 = 40 \mu\text{m}$, $d_4 = 80 \mu\text{m}$ and $d_5 = 160 \mu\text{m}$.

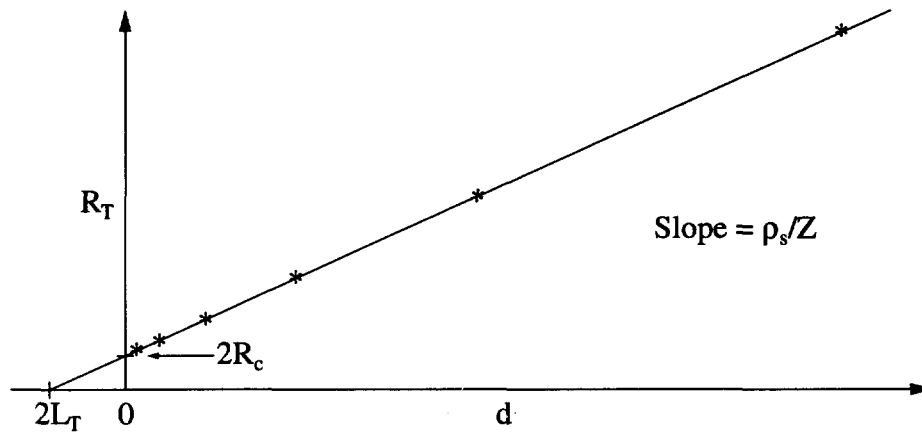


Fig. 5.1. A transfer length method test structure with dimensions and a plot of total resistance as a function of contact spacing d .

5.1.2. FABRICATION OF TLM STRUCTURES

The process steps to fabricate the Transfer length measurement (TLM) structures are shown in fig. 5.2. The measurement structures were formed in: (1) two, three layer $6\text{H}\alpha\text{-SiC}$ structures epitaxially grown on (0001) $6\text{H}\alpha\text{-SiC}$

substrates and (2) a three layer β -SiC structure epitaxially grown on (111) TiC substrate. The SiC epilayers were grown by chemical vapor deposition (CVD), using 1,2-disilylethane.¹¹³ First, three to four μm thick electrical isolation epilayers were synthesized by in-situ doping with boron during growth. Second, n^+ SiC epilayers, in-situ doped with nitrogen (N), were grown. Both n^+ $6H\alpha$ -SiC epilayers were approximately 1 μm thick, with nitrogen concentration ($[N]$) = $4 \times 10^{19}\text{cm}^{-3}$. This $[N]$ exceeds that which can be substitutionally incorporated into the SiC lattice, but is less than the maximum $[N]$ that can be accommodated by a single crystal SiC lattice.¹⁵ The n^+ β -SiC layer, was approximately 0.5 μm thick, with nitrogen concentration ($[N]$) = $2 \times 10^{19}\text{cm}^{-3}$ (see section 3.4).

TiC (111) contact epilayers, 1500 \AA thick, were grown on one of the n^+ - $6H\alpha$ -SiC epilayers and the n^+ β -SiC epilayer, by CVD, at 1260 $^\circ\text{C}$, using TiCl_4 and C_2H_4 (see section 4.3). A 1500 \AA thick, polycrystalline TiC contact layer was deposited on the other n^+ $6H\alpha$ -SiC epilayer by DC sputtering (see section 4.4.2).

An array of transmission line mesas was formed by selectively etching SiC on each structure by reactive ion etching (dry etching), using SF_6 . This dry etching technique was used because: (1) SiC does not respond to any conventional etchant even at high temperatures, owing to its chemical stability, (2) this technique gives highly anisotropic etching. In the next step, 6 equal area TiC Shockley pads were formed on each mesa (see Fig. 5.2). The CVD grown TiC Shockley pads were formed by photomasking and wet chemical etching (5000 $\text{\AA}/\text{hr.}$), using 5:1:4:: HNO_3 : H_2SO_4 : H_2O , at 40 $^\circ\text{C}$. The as-sputtered TiC Shockley pads on n^+ $6H\alpha$ -SiC were formed in 2 steps; first, about 1300 \AA of TiC was removed by reactive ion

etching (using SF_6), second, the remaining TiC between Shockley pads was removed as described above for CVD grown TiC. The reactive ion etching (RIE) step was necessary because the wet-etch rate of as-sputtered TiC was about 50 Å/hr.

The RIE caused surface leakage current on the side-walls of the TLM structures. This was eliminated by annealing in H_2 . The CVD grown TiC Shockley pads were passivated by annealing at 1300 °C, for 15 minutes. The side-walls of the TLM structures with sputtered TiC Shockley pads were passivated during the forming and annealing procedures.

Sputtered TiC contacts were formed and annealed, in H_2 , for a total time of 35 minutes (20 min. at 1255 °C and 15 min. at 1295 °C). There were altogether 5 anneal cycles. The effects of each of 5 anneal cycles were investigated by microscopic observation of the TiC surface texture, by I-V measurements as a function of Shockley pad spacing and by attempting to scratch the Shockley pad surfaces.

The contacts were annealed until they became hard and their pre and post anneal electrical properties were unchanged. The first three annealing cycles were performed at 1255 °C, for 5 min., 5 min. and 10 min. The as-sputtered fine grainy surface of the TiC Shockley pads remained unchanged by these anneal cycles. The I-V characteristics between Shockley pads were ohmic after the first anneal cycle, but the linearity of the total resistance (R_T) versus Shockley pad (d) spacing data improved and the specific contact resistance, decreased after each anneal cycle. The Shockley pads could be scratched after each of the first 3 anneal cycles.

The fourth and fifth annealing cycles were performed at 1295 °C, for 5 min.

and 10 min. The Shockley pad surfaces exhibited a flat, cracked-like surface after anneal 4. The R_T versus d data was linear after anneal 4 and the specific contact resistance was lower than after anneal 3. The Shockley pads could not be scratched after anneal 4. The contacts exhibited the same morphology, electrical and hardness properties before and after anneal 5. The significant change in the properties of the TiC contacts after anneal 4 indicates that a critical temperature for TiC crystallization and TiC/SiC interface reaction exists between 1255 °C and 1295 °C. The absence of change in the properties of the TiC contacts after anneal 5 suggests that the TiC/SiC interface reaction goes to completion rapidly, at a specific temperature, and thereafter, the interface is very stable at or below 1295 °C. Thus, it is likely that the forming and annealing process can be performed by rapid thermal annealing.

5.1.3. MEASUREMENT PROCEDURE

First, electrical isolation of the SiC layers was checked. This was done from the I-V curves obtained between probes on Shockley pads of adjacent TLM structure mesas, using a Tektronix 576 curve tracer.

All transfer length measurement data was obtained (at 300 °K) using an HP4145B semiconductor parameter analyzer; by measuring current versus voltage as a function of Shockley pad spacing. In order to accurately measure the total resistance between the Shockley pads and reduce error, the probe resistance was determined just before each TLM structure measurement and subtracted from the resistance measured between the Shockley pads. Caution was taken to ensure a good contact with between the probes and Shockley pads, by applying pressure to the probes and rubbing them on TiC surface. The best contact resulted in lowest possible observed resistance measurement. The Shockley pad dimensions and spacing, and the transmission line mesa dimensions were measured from 900x Nomarsky micrographs.

The sheet resistance ρ_s , contact resistance R_c , transfer length L_T , and specific contact resistance ρ_c , presented in Tables 6.2, 6.3 and 6.4, were determined from the Shockley pad dimensions and a linear curve obtained from the standard error of linear regression of the R_T data on d . These values were determined based on the theory of transfer length method described in section 5.1.1.

5.2. DETERMINATION OF STABILITY OF CVD TiC/SiC INTERFACE

The stability of TiC/SiC interface under high temperature conditions was

determined by examining thinned CVD TiC/SiC cross-section samples, using 200 KV Hitachi-800 transmission electron microscope (TEM), by Zhao et.al. The TEM samples were prepared following the conventional “sandwich method”. Slices were cut perpendicular to the interface using a low speed diamond saw. Two slices were then glued together using epoxy to form a sandwich with the TiC layers facing each other. The sandwich was mechanically thinned to about 20-30 μm and subsequently dimpled. Final thinning was performed with a 4 KeV Ar ion beam, until the TiC/SiC was perforated. The results observed are presented in the next chapter.

The stability of TiC/SiC interface under high current density conditions was determined by subjecting the ohmic contacts (shockley pads) to repetitive biasing at maximum compliance of the HP4145B (105 mA) for 1 hour, and observing any changes in the total resistance.

5.3. TEST OF HARDNESS AND ADHESION

The hardness and adhesion of TiC contacts was determined by using the following methods: (1) A tungsten-carbide scribe was used to scratch TiC contacts (after annealing in case of sputtered TiC). (2) Attempts were made (on a separate, but identically processed sample) to peel CVD grown TiC from a SiC surface, by bonding the TLM structure array surface to a thin stainless steel plate with epoxy, and then trying to separate the TLM structure array from the plate. The results of these tests are reported in the next chapter.

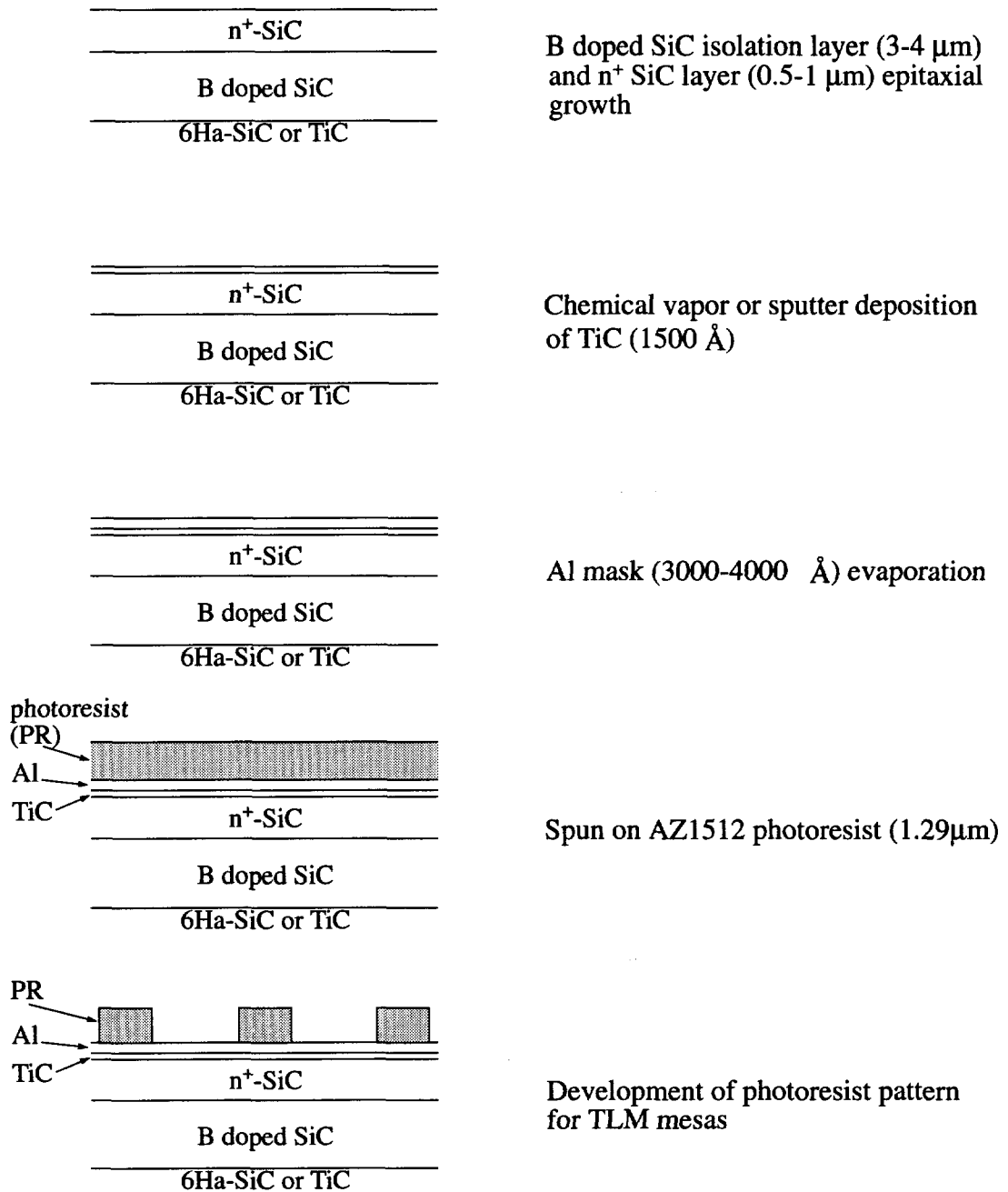
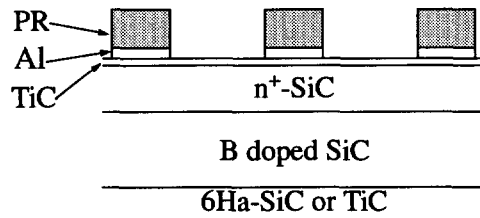
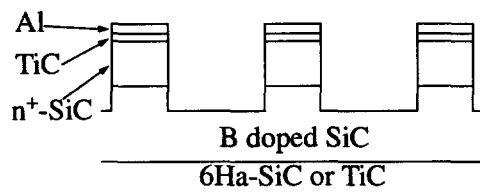
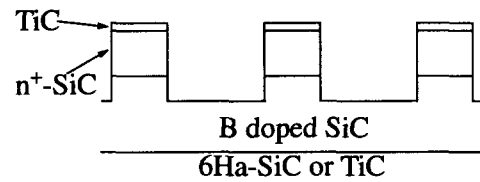


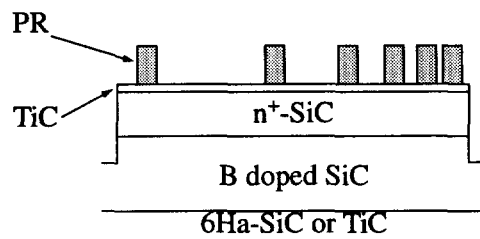
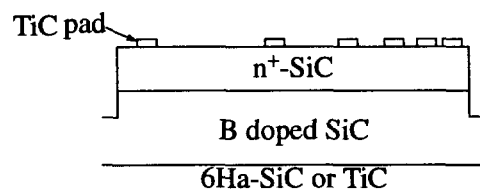
Fig. 5.2. Process steps for fabrication of TLM structures



Al etching

Reactive ion etching (SF_6)

TLM mesas after removal of Al mask

A TLM mesa rotated 90° , with S1818 ($2.05\ \mu\text{m}$) photoresist pattern for Shockley pads

TLM structure with six Shockley pads after TiC etching (dry or wet)

Fig. 5.2. Process steps for fabrication of TLM structures

CHAPTER 6

RESULTS & DISCUSSION OF OHMIC CONTACT CHARACTERIZATION

This chapter consists of the results and discussion of TiC ohmic contact characterization methods presented in chapter 5. Section 6.1 is on measurement of specific ohmic contact resistance by TLM, section 6.2 on determination of stability of TiC/SiC interface and section 6.3 on adhesion of TiC contacts to SiC.

6.1. MEASUREMENT OF SPECIFIC OHMIC CONTACT RESISTANCE

Measurement of specific ohmic contact resistance was carried out on CVD TiC contacts on n^+ 6H α -SiC (Sample A), sputtered TiC contacts on n^+ 6H α -SiC (sample B) and CVD TiC contacts on n^+ β -SiC (sample C). The TLM structures for all three sample are shown in Fig. 6.1. The following subsection presents the measurements results, comparison and discussion of the results of specific contact resistance measurements, i.e sputter deposited ohmic contacts versus chemical vapor deposited and ohmic contacts to β -SiC versus ohmic contacts to 6H α -SiC.

6.1.1. RESULTS AND DISCUSSION

Table 6.1 lists the dimensions of the transfer length measurement structures

obtained after photolithographic processing of the three samples. The Shockley pad dimensions differ from the photomask dimensions ($L = 30 \mu\text{m}$ and $Z = 90 \mu\text{m}$) because of TiC wet etchant undercutting/over etching at the photoresist/TiC interface during Shockley pad etching. However, the Shockley pad boundaries remained acceptably defined (Fig. 6.2 (a), (b) and (c)).

The Shockley pads on sample C were $17 \mu\text{m}$ long (L) x $77 \mu\text{m}$ wide (Z), at their widest point. The rounding of the Shockley pad ends was corrected for by using $Z = 75 \mu\text{m}$.

Table 6.1: Dimensions obtained after fabrication of TLM structures.

TLM Structure	Transmission line mesa dimension (L).(W).(H) (μm)	Shockley pad dimension (L).(Z) (μm)	Shockley pad spacing (μm)				
			d_{12}	d_{23}	d_{34}	d_{45}	d_{56}
A	530 x 100 x 2.4	25 x 85	15	25	45	85	165
B	530 x 100 x 2.4	29.75 x 87.7	10.5	20.5	40.5	80.5	160.5
C	530 x 100 x 2.5	17 x 77	23	33	53	93	173

The electrical isolation of the SiC layers was found to be adequately high for the purpose of Transfer length method measurements. The resistance between TLM structure mesas on sample A was greater than 10^5 ohms, from 0 to 10 volts. The leakage current between TLM structure mesas on sample B was less than $0.1 \mu\text{A}$ at 7 volts, and less than $1 \mu\text{A}$ at 10 volts. The resistance between TLM structure mesas on sample C was greater than 10^6 from 0 to 3 volts.

The current between Shockley pads, measured to the maximum compliance

of the HP4145B (105 mA), was a linear function of applied voltage. This demonstrated that the contacts are ohmic. The average values of R_T versus d , obtained from 17 TLM structures on A, 10 TLM structures on B and 10 TLM structures on C are plotted in Fig. 6.3, Fig. 6.4 and Fig. 6.5, respectively. The individual and average values of ρ_s , R_c , L_T and ρ_c for sample A, B and C are presented in the Tables 6.2 (A), 6.3 (B) and 6.4 (C).

The differences in the R_T versus d slopes, indicated by ρ_s in the Tables, are thought to be due to thickness differences in SiC epilayers at different TLM structure positions. These thicknesses were $\approx 1.0 \pm 0.05 \mu\text{m}$ for $6\text{H}\alpha\text{-SiC}$ samples and $0.5 \pm 0.025 \mu\text{m}$ for $\beta\text{-SiC}$ sample. The thicknesses in the center were used to calculate resistivity values of the n^+ SiC epilayers.

The resistivity value obtained for sample A was $\approx 1.34 \times 10^{-3} \Omega \cdot \text{cm}^{-3}$, for sample B was $\approx 8.74 \times 10^{-4} \Omega \cdot \text{cm}^{-3}$ and for sample C was $\approx 8.08 \times 10^{-3} \Omega \cdot \text{cm}^{-4}$. The difference in resistivity calculated for A and B may be due to the higher leakage current in A and/or a difference in the sheet resistance under the epitaxial and polycrystalline TiC contacts. The calculated resistivity values of the n^+ $6\text{H}\alpha\text{-SiC}$ epilayers agree within a factor of 2, and indicate that $\rho \approx 1 \times 10^{-3} \Omega \cdot \text{cm}$ in n^+ $6\text{H}\alpha\text{-SiC}$ as doped in this study.

The resistance between Shockley pads (R_T) for sample A and B, increased linearly with spacing (d), but for sample C, the linear increase was only for measurements between Shockley pads 2-3, 3-4, 4-5, and 5-6. The value of R_T between Shockley pads 1-2 is slightly above the straight line curve through R_{23} , R_{34} , R_{45} and R_{56} . This is because the added resistance of the longer current path length

between the rounded Shockley pad ends, as opposed to between facing Shockley pad edges, becomes a larger fraction of the total resistance as the Shockley pad spacing becomes shorter.

A very high value of correlation coefficient for a straight line curve fit to the measured R_T versus d data, for each TLM structure, was observed. It was better than 0.998 for CVD TIC/ n^+ 6H α -SiC sample, better than 0.9994 for sputtered TIC/ n^+ 6H α -SiC sample and CVD TIC/ n^+ β -SiC sample. The average of the correlation coefficient, was 0.9994 for the 17 measured structures of TIC/ n^+ 6H α -SiC sample, 0.9997 for the 10 measured structures of sputtered TIC/ n^+ 6H α -SiC sample and 0.9998 for the 10 measured structures of CVD TIC/ n^+ β -SiC sample.

The maximum error - determined from the standard error of linear regression of R_T on d - in the extrapolated values of R_c and L_T , used to calculate ρ_c for A, was less than $\pm 2.4\%$. This indicates an uncertainty in the average value of ρ_c of about 4.8%. This suggests that the correct value of ρ_c is within the range $1.24 \times 10^{-5} \Omega \cdot \text{cm}^2 < \rho_c < 1.36 \times 10^{-5} \Omega \cdot \text{cm}^2$.

The maximum error in the extrapolated values of R_c and L_T , used to calculate ρ_c for B, was less than $\pm 2\%$. This indicates an uncertainty in the average value of ρ_c of about 4% and suggests that the correct value of ρ_c is within the range $2.8 \times 10^{-5} \Omega \cdot \text{cm}^2 < \rho_c < 3 \times 10^{-5} \Omega \cdot \text{cm}^2$.

The maximum error in the extrapolated values of R_c and L_T , used to calculate ρ_c for C, was about $\pm 9\%$. This indicates an uncertainty in the average value of ρ_c of about 18% and suggests that the correct value of ρ_c is within the range $4.46 \times 10^{-6} \Omega \cdot \text{cm}^2 < \rho_c < 6.42 \times 10^{-6} \Omega \cdot \text{cm}^2$.

The average transfer length for epitaxial TiC/n⁺ 6H α -SiC contacts was 9.5 μm and for sputtered TiC/n⁺ 6H α -SiC was 17 μm . The epitaxial grown TiC contacts exhibited about 44% shorter L_T and about 18% lower R_c than the sputtered TiC contacts. The average specific contact resistance of epitaxial TiC contacts¹³³ ($1.30 \times 10^{-5} \Omega \cdot \text{cm}^2$) was about 55% lower than sputtered TiC contacts¹³⁵ ($2.89 \times 10^{-5} \Omega \cdot \text{cm}^2$). It is possible that the sputtered TiC contact properties could be improved by optimized process development; however, the results obtained here suggest that interface state reduction at the epitaxial TiC/6H α -SiC interface may contribute to lower ρ_c values.⁹³

The average transfer length for epitaxial TiC/n⁺ β -SiC contacts was 5.0 μm . The average specific contact resistance of epitaxial TiC/n⁺ β -SiC contacts¹³⁵ ($5.44 \times 10^{-6} \Omega \cdot \text{cm}^2$) was 60% lower than epitaxial TiC/n⁺ 6H α -SiC contacts. This value is in accordance with superior transport properties of β -SiC. An approximate theoretical calculation of the relative current densities through the two types of single crystal epitaxial CVD TiC contacts, can be made assuming that contacts are ideal in nature (because of reduced interface state density). The ideal nature causes an accumulation type of ohmic contact¹⁰⁸ to form which is desirable because of absence of any energy barrier to transport of majority carriers (in either direction in this particular case, see Fig. 7.1). The approximate ratio of current densities at the same applied bias, neglecting the difference in electron affinity, dielectric constant and carrier concentration for the two types of polytypes, is:

$$\frac{J_n(\beta)}{J_n(\alpha)} = \frac{D_n(\beta) N_c(\beta)}{D_n(\alpha) N_c(\beta)} = \frac{\mu_n(\beta) \left(\frac{m_{de}(\beta)}{m_{de}(\alpha)} \right)^{3/2}}{\mu_n(\alpha) \left(\frac{m_{l(\beta)} m_{l(\beta)}^2}{m_{l(\alpha)} m_{l(\alpha)}^2} \right)^{1/2}} \quad (6.1)$$

where J is current density, D is diffusion constant, N_c is density of states at the conduction band, μ is drift mobility, m_{de} is density of state effective mass for electrons, m_l is longitudinal effective mass of electron and m_t is transverse effective mass of electron. The effective masses are in units of rest mass. The subscripts α and β denote the polytypes of SiC and n denotes the majority carrier electron. Substituting appropriate values of the physical quantities¹³⁶ we get:

$$\frac{J_{n(\beta)}}{J_{n(\alpha)}} = \frac{(\mu_{n(\beta)} \geq 750)}{(\mu_{n(\alpha)} \approx 250)} \left(\frac{0.677 \cdot 0.247^2}{1.5 \cdot 0.25^2} \right)^{1/2} \geq 2 \quad (6.2)$$

The substituted value of drift mobility of electrons in 6H α -SiC is typical of moderately doped ($\approx 10^{17}$ /cm³) layers.⁴ The substituted value (750 cm²/Vs) of drift mobility of electrons in β -SiC is a conservative estimate because it is a value in β -SiC layers grown on Si substrates which have high density of defects due to large lattice parameter mismatch.^{37,40} Assuming approximately same degradation of mobility for both polytypes when doped degenerately, it is seen that the value obtained in equation 7.2 agrees with the ratio of specific contact resistances, $\rho_{c(\alpha)}/\rho_{c(\beta)} = 2.4$, for the two polytypes obtained by measurement.

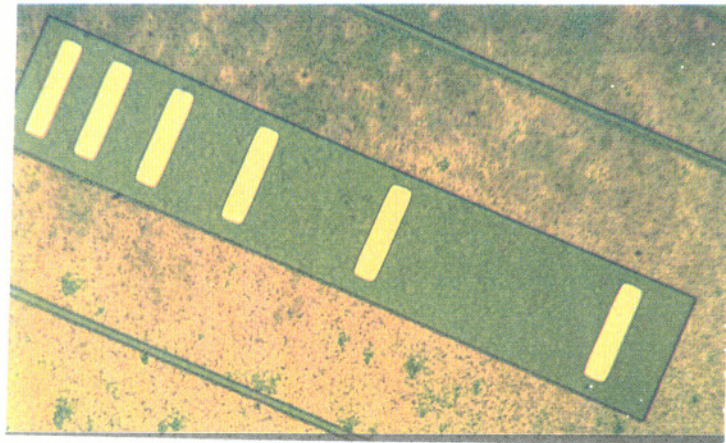
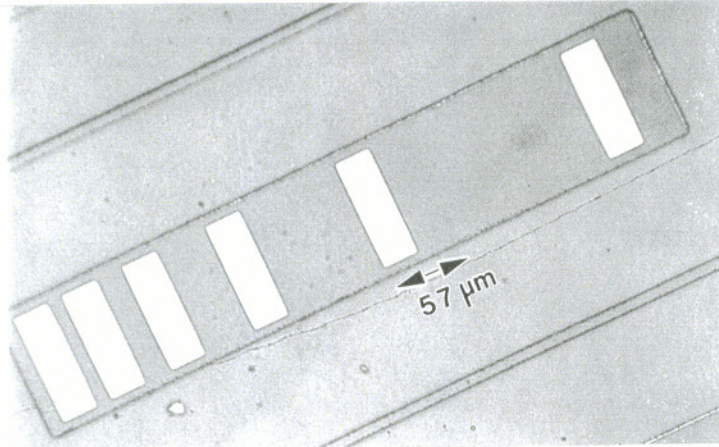
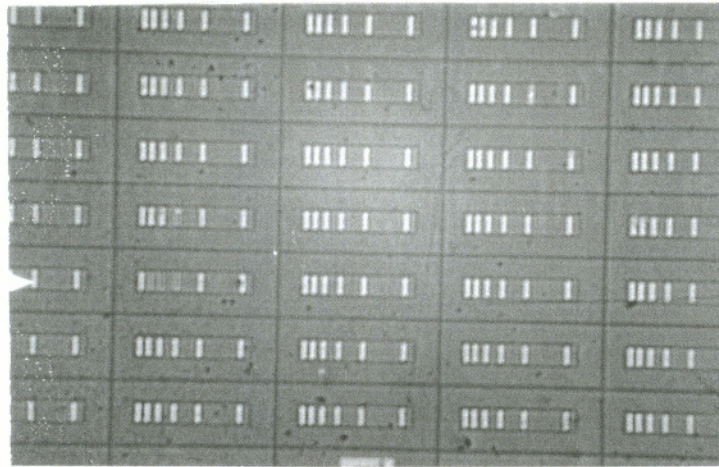


Fig. 6.1. TLM structure on (a) sample A, (b) sample B and (c) sample C, showing TiC Shockley pads; light areas are TiC, dark area is n^+ SiC.

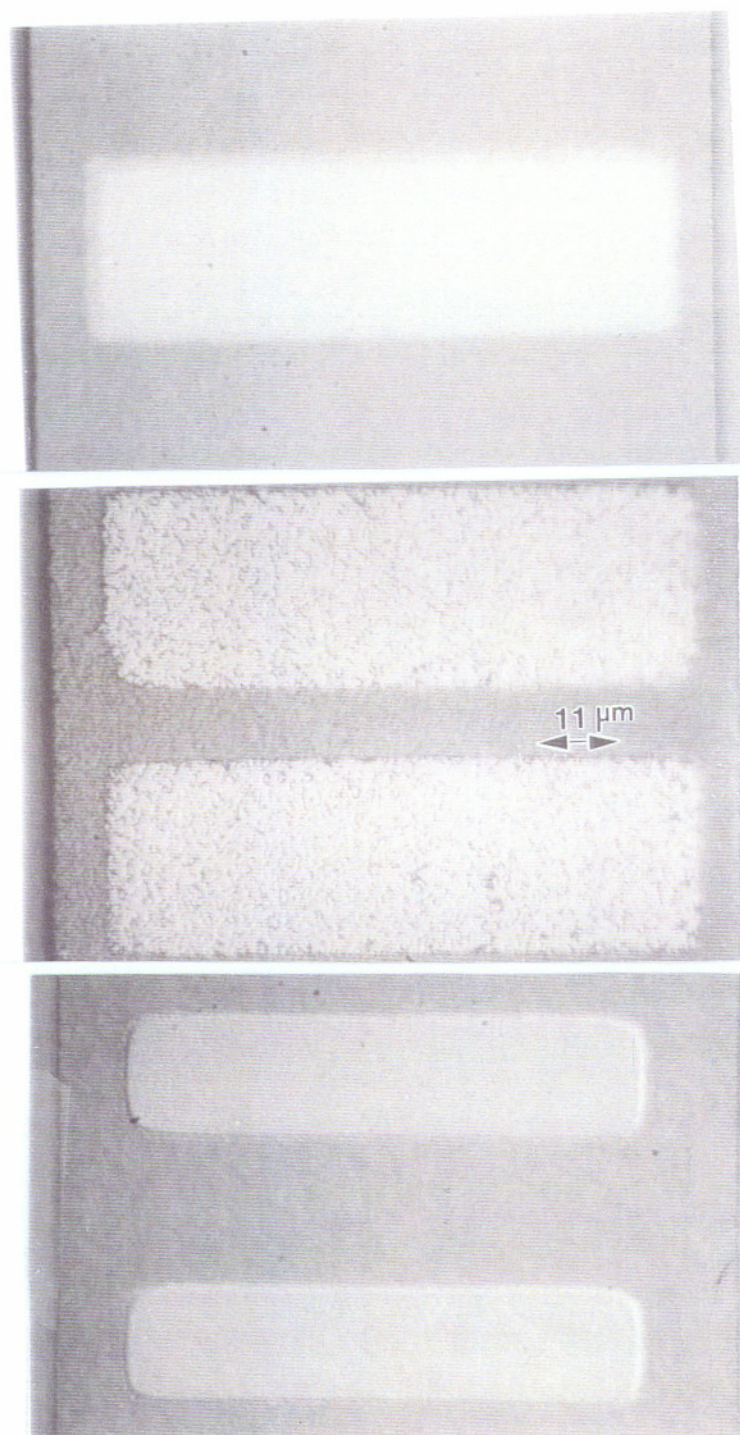


Fig. 6.2. TiC Shockley pad dimensions and mesa width on (a) sample A, (b) sample B (annealed) and (c) sample C.

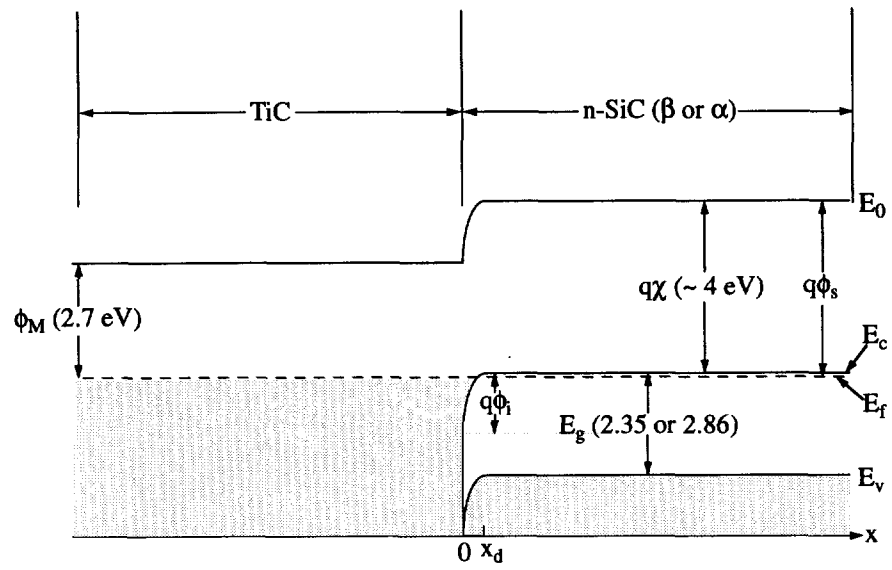


Fig. 6.3. Equilibrium band diagram of ideal TiC/n-SiC (degenerately doped) accumulation type ohmic contact.

Table 6.2: Transfer length measurement data and calculations (CVD TiC/ n⁺ 6H α -SiC).

TLM#	R ₁₂ (ohm)	R ₂₃ (ohm)	R ₃₄ (ohm)	R ₄₅ (ohm)	R ₅₆ (ohm)	Linear curve fit (R _T on d)			R _c (ohm)	L _T (cm)	ρ_c (ohm-cm ²)
						corr. coeff.	Std. error (ohm)	R _s (ohm/sq)			
F13	5.40	6.35	9.94	15.90	28.87	0.9996	0.2638	13.42	1.36	0.00086	9.91 x 10 ⁻⁶
F7	6.54	8.53	11.20	18.48	32.31	0.9997	0.2766	14.59	1.96	0.00114	1.89 x 10 ⁻⁵
E15	4.68	6.52	9.50	15.28	25.17	0.9985	0.4488	11.51	1.58	0.00116	1.56 x 10 ⁻⁵
F8	5.94	7.70	10.77	17.98	31.70	0.9999	0.1501	14.63	1.64	0.00095	1.33 x 10 ⁻⁵
G12	5.85	7.00	11.02	17.77	30.96	0.9996	0.2727	14.36	1.60	0.00095	1.29 x 10 ⁻⁵
G10	5.20	6.83	10.04	16.56	30.33	0.9999	0.1580	14.24	1.29	0.00077	8.38 x 10 ⁻⁶
G11	6.16	8.35	12.32	18.42	33.09	0.9994	0.3867	15.04	1.91	0.00108	1.75 x 10 ⁻⁵
H11	5.45	6.90	10.62	17.00	30.47	0.9999	0.1449	14.20	1.45	0.00087	1.07 x 10 ⁻⁵
F9	5.87	7.56	11.05	17.31	31.27	0.9998	0.1967	14.34	1.65	0.00098	1.38 x 10 ⁻⁵
G5	6.38	7.97	11.45	19.10	33.21	0.9999	0.1778	15.31	1.78	0.00099	1.49 x 10 ⁻⁵
G7	5.21	7.63	10.38	18.44	31.73	0.9991	0.4445	14.98	1.44	0.00082	9.96 x 10 ⁻⁶
E4	5.43	7.35	10.74	15.32	29.24	0.9976	0.6566	13.22	1.60	0.00103	1.40 x 10 ⁻⁵
E7	5.52	7.57	10.82	16.53	29.41	0.9996	0.2672	13.35	1.72	0.00110	1.61 x 10 ⁻⁵
F10	4.97	7.40	11.88	17.24	32.04	0.9980	0.6804	14.96	1.46	0.00083	1.02 x 10 ⁻⁵
H7	6.11	7.90	11.62	18.80	33.31	1.0000	0.0357	15.41	1.70	0.00094	1.36 x 10 ⁻⁵
H15	6.12	7.73	11.49	19.34	33.90	0.9999	0.1795	15.85	1.61	0.00086	1.18 x 10 ⁻⁵
H13	5.40	7.33	11.13	18.85	32.17	0.9993	0.4004	15.19	1.50	0.00084	1.07 x 10 ⁻⁵
Average	5.66	7.45	10.94	17.55	31.13	0.9994	0.0759	14.39	1.60	0.00095	1.30 x 10 ⁻⁵

Table 6.3: Transfer length measurement data and calculations (sputtered TiC/ n⁺ 6H α -SiC).

TLM#	R ₁₂ (ohm)	R ₂₃ (ohm)	R ₃₄ (ohm)	R ₄₅ (ohm)	R ₅₆ (ohm)	Linear curve fit (R _T on d)			R _s (ohm/sq)	R _c (ohm)	L _T (cm)	ρ_c (ohm-cm ²)
						corr. coeff.	std. error (ohm)					
I19	4.79	5.63	7.64	11.97	19.61	0.9997	0.1520	8.74	1.85	0.00185	3.00 x 10 ⁻⁵	
E20	4.43	5.71	7.42	11.58	19.65	0.9998	0.1189	8.84	1.73	0.00171	2.59 x 10 ⁻⁵	
J19	4.29	5.33	7.58	11.53	20.08	0.9999	0.0904	9.20	1.60	0.00153	2.14 x 10 ⁻⁵	
E17	4.12	5.12	7.01	11.52	19.98	0.9998	0.1174	9.32	1.45	0.00137	1.74 x 10 ⁻⁵	
I16	4.99	5.63	8.04	11.90	20.55	0.9996	0.1901	9.17	1.84	0.00176	2.86 x 10 ⁻⁵	
F12	5.43	6.57	8.33	13.17	21.87	0.9996	0.1855	9.66	2.10	0.00190	3.5 x 10 ⁻⁵	
G9	6.11	6.90	9.55	14.13	22.69	0.9995	0.2102	9.79	2.45	0.00220	4.72 x 10 ⁻⁵	
G15	4.54	5.68	8.57	12.86	22.34	0.9996	0.2125	10.359	1.71	0.00145	2.17 x 10 ⁻⁵	
H8	5.48	6.59	9.32	15.51	26.50	0.9997	0.2173	12.43	1.91	0.00135	2.26 x 10 ⁻⁵	
D8	7.69	9.18	12.52	20.06	32.66	0.9994	0.3553	14.74	2.96	0.00176	4.57 x 10 ⁻⁵	
Average	5.19	6.23	8.60	13.42	22.59	0.9997	0.0794	10.22	1.96	0.00168	2.89 x 10 ⁻⁵	

Table 6.4: Transfer length measurement data and calculations (CVD TiC/ n⁺ β-SiC).

TLM#	R ₁₂ (ohm)	R ₂₃ (ohm)	R ₃₄ (ohm)	R ₄₅ (ohm)	R ₅₆ (ohm)	Linear curve fit (R _T on d)		R _s (ohm/sq)	R _c (ohm)	L _T (cm)	ρ _c (ohm-cm ²)
						corr. coeff.	Std. error (ohm)				
G20	7.58	9.33	12.70	21.87	39.12	0.9996	0.3868	16.15	0.90	0.00042	2.83 x 10 ⁻⁶
E19	8.56	10.92	14.45	23.24	40.56	0.9997	0.3174	16.03	1.74	0.00082	1.07 x 10 ⁻⁵
G9	9.18	11.88	17.09	29.70	51.97	0.9997	0.4590	21.62	1.15	0.00040	3.43 x 10 ⁻⁶
J9	8.34	10.58	16.64	26.66	45.93	0.9994	0.5361	18.74	1.48	0.00059	6.61 x 10 ⁻⁶
I8	9.89	11.99	17.38	27.50	49.04	0.9999	0.2037	19.81	1.61	0.00061	7.40 x 10 ⁻⁶
F10	9.86	12.88	18.48	29.63	52.90	0.9999	0.1891	21.45	1.65	0.00058	7.14 x 10 ⁻⁶
G8	11.00	13.90	19.56	31.77	54.50	0.9999	0.2637	21.80	2.18	0.00075	1.23 x 10 ⁻⁵
G7	10.58	13.82	19.65	33.94	60.87	0.9998	0.4059	25.41	1.13	0.00033	2.82 x 10 ⁻⁶
F8	11.70	14.74	22.47	37.68	65.79	0.9998	0.4992	27.28	1.58	0.00043	5.14 x 10 ⁻⁶
E9	12.15	15.85	22.84	39.49	71.48	0.9999	0.6343	30.01	1.10	0.00027	2.27 x 10 ⁻⁶
Average	9.88	12.59	18.13	30.15	53.22	0.9998	0.2573	21.83	1.45	0.00050	5.44 x 10 ⁻⁶

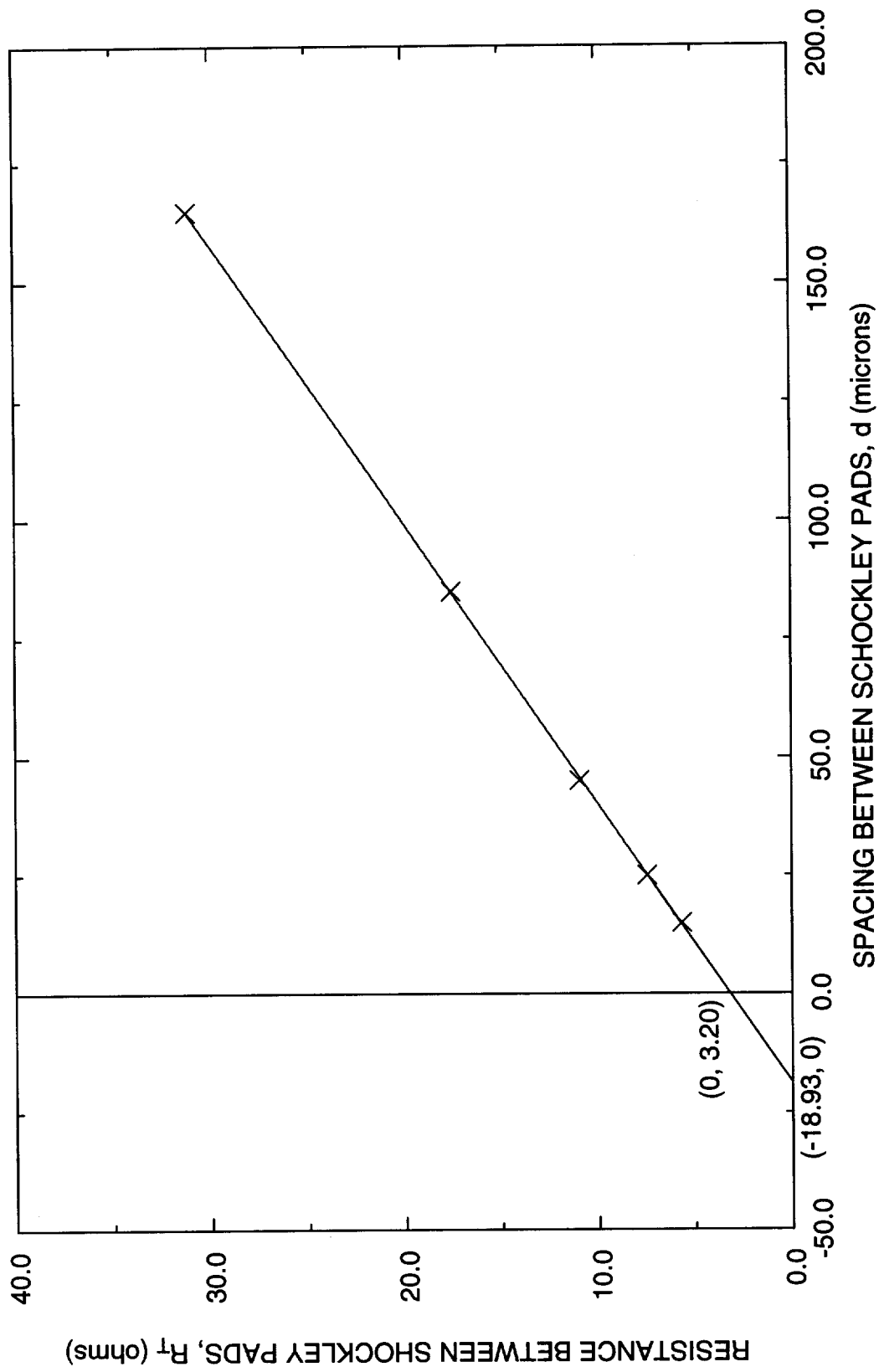


Fig. 6.4. Average resistance between Shockley pads versus spacing for CVD TiC/n-type 6H α -SiC.

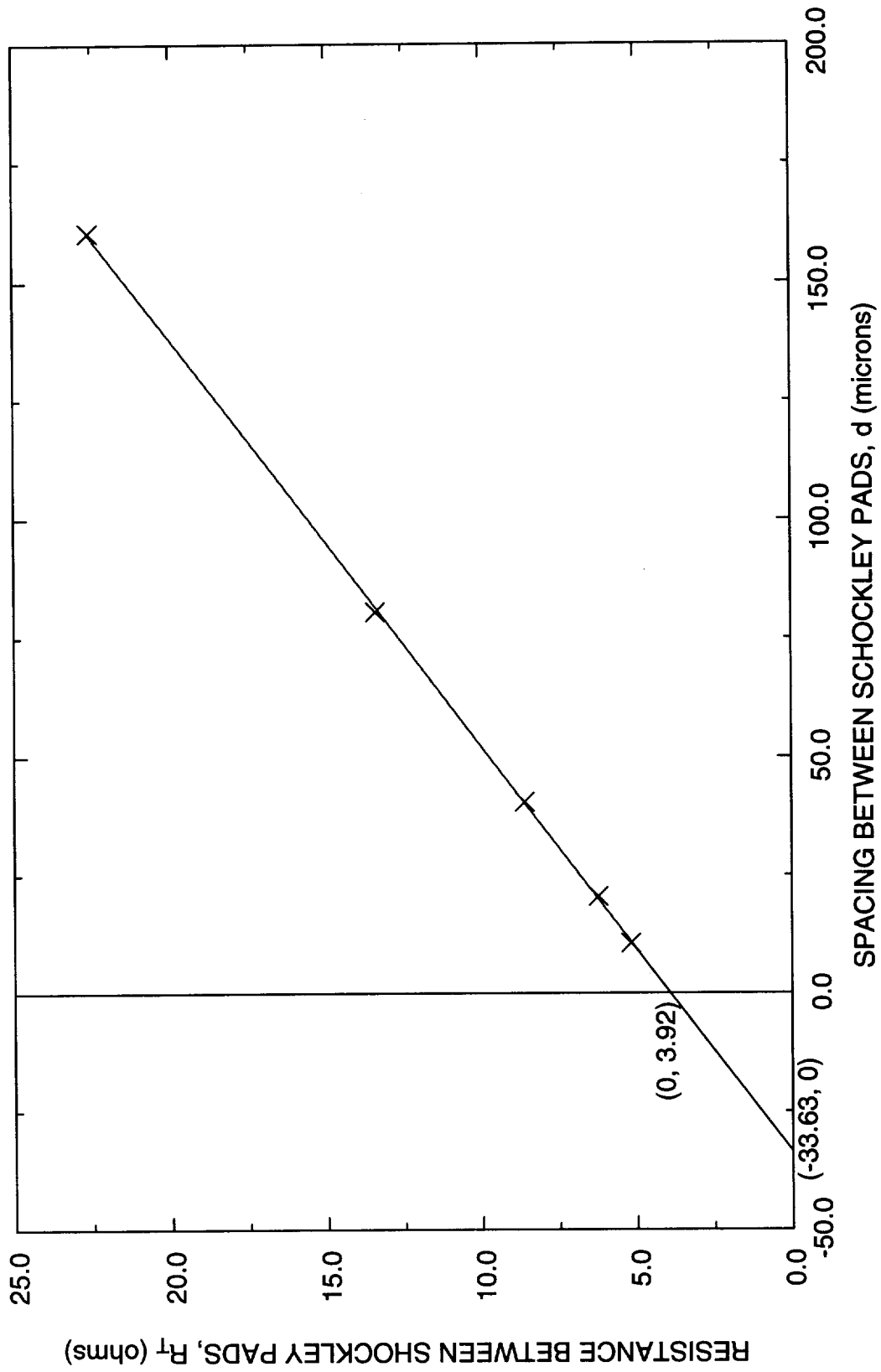


Fig. 6.5. Average resistance between Schottky pads versus spacing for sputtered TiC/n-type 6H α -SiC.

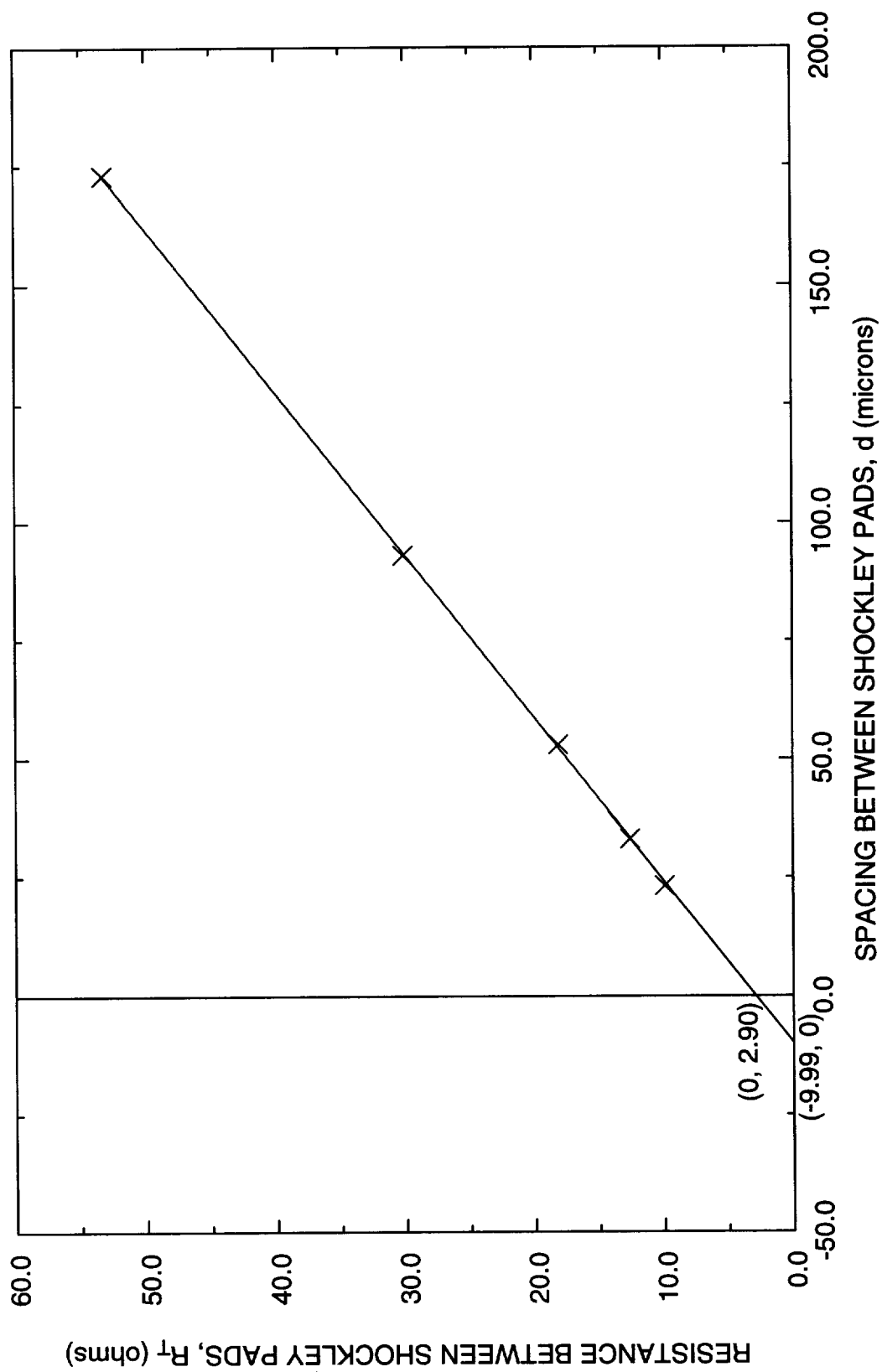


Fig. 6.6. Average resistance between Shockley pads versus spacing for CVD TiC/n-type β -SiC.

6.2. DETERMINATION OF STABILITY OF TiC/SiC INTERFACE

6.2.1. RESULTS AND DISCUSSION

T.E.M. examination of the CVD TiC/SiC interface shows that the interface is abrupt, there is no interdiffusion and also no formation of any third phase (see Fig. 6.7 (a) and (b)). The only electron diffraction patterns obtained in the vicinity of the interface were that of TiC or SiC. The pictures shown are representative of entire interface examined.

The I-V characteristics and hence total resistance between Shockley pads remained unchanged when repetitively biased to maximum compliance of the HP4145B (105 mA) for 1 hour. The maximum current density through the contact areas of A, B and C was greater than 4,700, 4,100 and 7,800 amps/cm², respectively (based on the total Shockley pad areas). It was greater than 9,000, 7,400 and 19,100 amps/cm², respectively, within the L_T.Z.SP (Shockley pad area).

6.3. RESULTS OF TEST OF HARDNESS AND ADHESION

The CVD as well as annealed sputter deposited TiC contacts could not be scratched by tungsten carbide scriber. Further, CVD TiC contacts, bound to stainless steel plate by epoxy, could not be delaminated from the SiC surface.

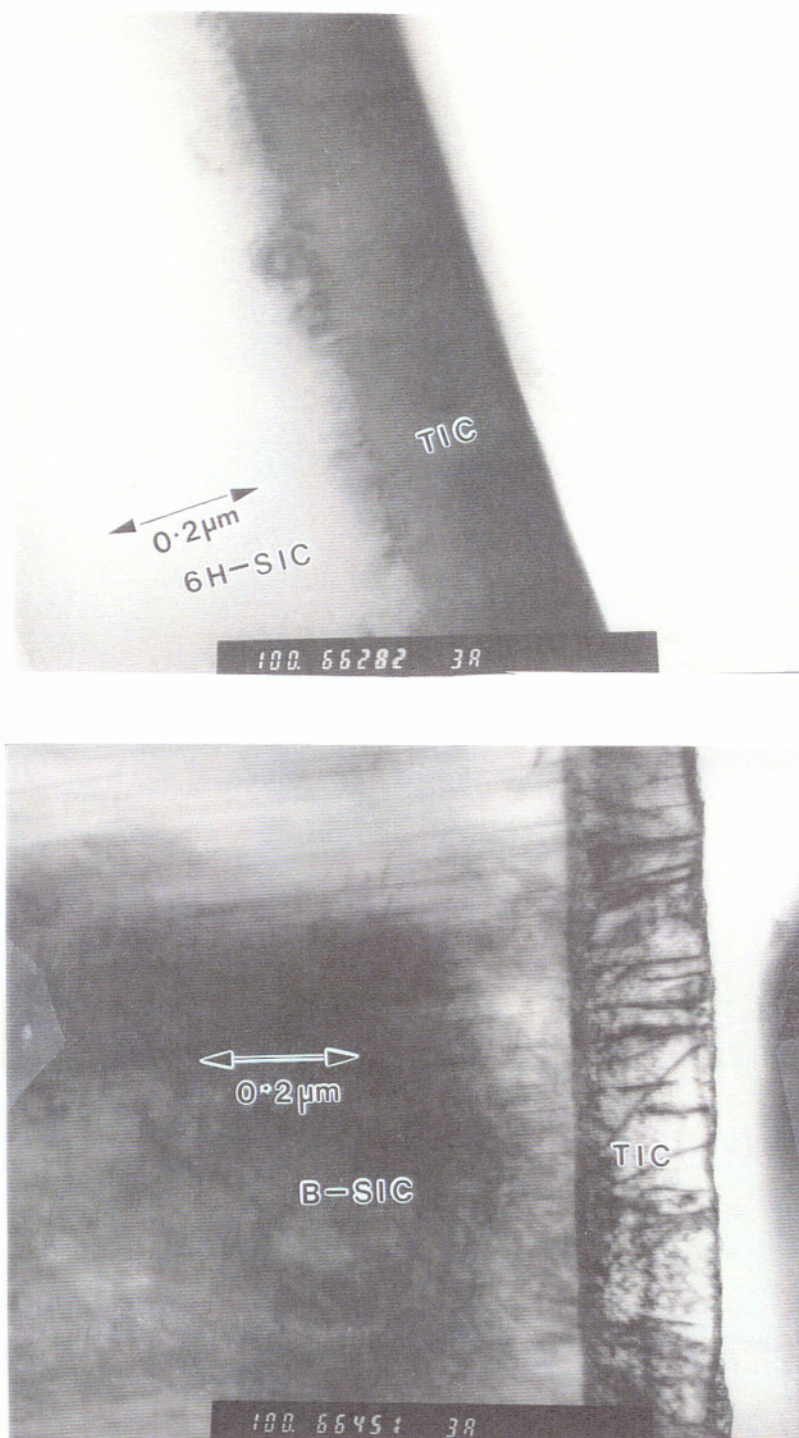


Fig. 6.7. XTEM micrographs showing (a) epitaxial CVD TiC/6H α -SiC interface and (b) epitaxial CVD TiC/ β -SiC interface.

CHAPTER 7

CONCLUSIONS

7.1. CONCLUSIONS

TiC ohmic contact metallization to n-type SiC was developed and characterized. TiC ohmic contacts were formed by sputter deposition and metal-organic chemical vapor deposition. Sputter deposition resulted in polycrystalline contacts while MOCVD in epitaxial single crystalline contacts.

The electrical properties of ohmic contacts were characterized by Transfer length method. The specific contact resistances obtained for epitaxial TiC contacts in this study, are the lowest reported for both n-type 6H α -SiC and β -SiC ohmic contacts (see table 2.3). The average specific contact resistance of epitaxial TiC/n⁺ 6H α -SiC contacts¹³³ was $1.30 \times 10^{-5} \Omega \cdot \text{cm}^2$ and of sputtered TiC/n⁺ 6H α -SiC contacts¹³⁵ was $2.89 \times 10^{-5} \Omega \cdot \text{cm}^2$. It is possible that the sputtered TiC contact properties could be improved by optimized process development; however, the results obtained here suggest that interface state reduction at the epitaxial TiC/6H α -SiC interface may contribute to lower ρ_c values.⁹³ The average specific contact resistance of epitaxial TiC/n⁺ β -SiC contacts¹³⁵ was $5.44 \times 10^{-6} \Omega \cdot \text{cm}^2$. This is 60% lower than epitaxial TiC/n⁺ 6H α -SiC contacts. This value is in accordance with superior transport properties of β -SiC.

Transfer lengths of ohmic contacts to n-type SiC are reported for the first time. The average transfer length for epitaxial TiC/n⁺ 6H α -SiC contacts was 9.5 μm , for sputtered TiC/n⁺ 6H α -SiC contacts was 17 μm and for epitaxial TiC/n⁺ β -SiC contacts was 5.0 μm .

The high temperature and high power stability of TiC/6H α -SiC and TiC/ β -SiC interfaces were excellent. The interfaces were stable at temperatures as high as 1250 °C and current density as high as 19000 Amps/cm².

The adhesion properties of the TiC contacts on SiC were outstanding.

REFERENCES

- 1 R.W. Keys, "Figure of merit for semiconductor high speed switches," *Proc. IEEE*, 60 (1), 225 (1972).
- 2 R.W. Keys, "Power dissipation in information processing," *Science*, 168, 796 (1970).
- 3 R.W. Keys, "Physical problems and limits in computer logic," *IEEE spectrum*, 6 (5), 35 (1969).
- 4 R.J. Trew, Y.B. Yan and P.M. Mock, "The potential of diamond and SiC electronic devices for microwave and millimeter-wave power applications," *Proc. IEEE*, 79 (5), 598 (1991).
- 5 M.G. Spencer, "The prospects of beta silicon carbide materials and devices," *Proc. 1991 Int. Semiconductor Device Res. Symp.* (Charlottesville, VA), 503 (1991).
- 6 B.J. Baliga, "Impact of SiC on power devices," *Amorphous and Crystalline Silicon Carbide IV*, Eds. C.Y. Yang, M.M. Rahman and G.L. Harris, Berlin: Springer-Verlag, 305 (1992).
- 7 P.A. Ivanov and V.E. Chelnokov, "Recent developments in SiC single crystal electronics," *Semiconductor Sci. Technol.*, 7, 863 (1992).
- 8 J.A. Powell and L.G. Matus, "Recent developments in SiC (USA)," *Amorphous and Crystalline Silicon Carbide*, Springer Proceedings in Physics, Eds. G.L. Harris and C.Y. Yang, 34, 2 (1989).
- 9 Y.M. Tairov and V.F. Tavetkov, "General principles of growing large-size single crystals of various silicon carbide polytypes," *J. Cryst. Growth*, 52, 146 (1981).
- 10 G. Zeigler, P. Lanig, D. Theis and C. Weyrich, "Single crystal growth of SiC substrate material for blue light emitting diodes," *IEEE Trans. Electr. Dev.*, ED-30, 227 (1983).
- 11 C.H. Carter, Jr., L. Tang and R.F. Davis, "Growth of single crystal boules of

α (6H)-SiC," presented at the *Fourth National Review Meeting on the Growth and Characterization of SiC*, Raleigh, NC, June 19, 1987.

- 12 H.S. Kong, J.T. Glass and R.F. Davis, "Chemical vapor deposition and characterization of 6H α -SiC thin films on off-axis 6H α -SiC substrates," *J. Appl. Phys.*, 64 (5), 2672 (1988).
- 13 S. Nishino, J.A. Powell and H.A. Will, "Production of large-area single-crystal wafers of cubic SiC for semiconductor devices," *Appl. Phys. Lett.* 42 (5), 460 (1983).
- 14 H.S. Kong, J.T. Glass and R.F. Davis, "Growth rate, surface morphology, and defect microstructures of β -SiC films chemically vapor deposited on 6H α -SiC substrates," *J. Mater. Res.*, 4 (1), 204 (1989).
- 15 J.D. Parsons, "Single crystal epitaxial growth of beta silicon carbide for device and integrated circuit applications," *Novel Refractory Semiconductors, Material Res. Soc. Symp. Proc.*, 97, 271 (1987).
- 16 R.F. Bunshah, J.D. Parsons, O.M. Stafsudd, "Wafer base for silicon carbide semiconductor device," U. S. Patent No. 4,767,666 (8/30/1988).
- 17 D.W. Brown and J.D. Parsons, "Chemical vapor deposition of silicon carbide," U.S. Patent No. 4,923,716 (5/8/1990).
- 18 J. Yang, P. Pirouz and J.A. Powell, "Stress induced defects vs. growth faults in CVD grown SiC," *Amorphous and Cryst. SiC and Related Materials II*, Ed. Rehman et al., Berlin: Springer-Verlag, 118 (1989).
- 19 P. Pirouz, C.M. Chorney and J.A. Powell, "Antiphase boundaries in epitaxially grown β -SiC," *Appl. Phys. Lett.*, 50 (4), 221 (1987).
- 20 A. Taylor and R.M. Jones, "Crystal structure and thermal expansion of cubic and hexagonal silicon carbide," *Silicon Carbide, Proc. Conf.*, Boston, Eds. J. R. O'Connor and J. Smithens, Pergamon Press, 147 (1960).
- 21 A.R. Verma and P. Krishna, *Polymorphism and Polytypism in Crystals*, John Wiley & Sons, New York, 1966.
- 22 Z. Inoue, H. Komatsu, H. Tanaka and Y. Inomata, "A new polytype of silicon

- carbide," *Proc. 3rd Int. Conf. on SiC*, Miami Beach, FL, 191 (1973).
- 23 C. Kittel, *Introduction to Solid State Physics*, Sixth ed., John Wiley & Sons, New York, 1986.
 - 24 G.R. Fisher and P. Barnes, "Towards a unified view of polytypism in silicon carbide," *Philos. Mag. B*, 61 (2), 217 (1990).
 - 25 Y.M. Tairov and Y.A. Vodakov, "Group IV materials (mainly SiC) (for electroluminescent devices)," in *Electroluminescence*, Ed. by J.I. Pankove Springer -Verlag, Berlin Heidelberg, New York, 31 (1977).
 - 26 L.A. Hemstreet and C.Y. Fong, "Recent band structure calculation of cubic and hexagonal polytypes of silicon carbides," in *Proc. 3rd Int. Conf. on SiC*, Miami beach, FL, 284 (1973).
 - 27 H.R. Philipp and E.A. Taft, "Intrinsic optical absorption in single crystal silicon carbide," in *SiC, A High Temperature semiconductor*," Ed. J.R. O'Connor and J. Smithens, Pergamon Press, 366 (1960).
 - 28 S.M. Sze, *Physics of Semiconductor Devices*, Second ed., John Wiley & Sons, New York, 1981.
 - 29 S.M. Sze and J.C. Irwin, "Resistivity, mobility and impurity levels in GaAs, Ge and Si at 300 °K," *Sol. St. Electron.*, 11, 599 (1968).
 - 30 W.E. Nelson, et. al., "Beta silicon carbide and its potential for devices," contract No. Nobsr-87235, DDC AD-428005 (12/13/1963).
 - 31 G.N. Violina, et. al., "Optical absorption and elec. properties of n-type α -SiC," *Sov. Phys. -Solid State*, 5 (12), 2500 (1964).
 - 32 M. Yamanaka, H. Diamon, E. Sakuma, S. Misawa and S. Yoshida, "Temperature dependance of electrical properties of n-type and p-type 3C-SiC," *J. Appl. Phys.*, 81 (2), 599(1987).
 - 33 J.A.W. Van Der DOES De BYE, "Transient recombination in silicon carbide," *Phillips Res. Repts.*, 17 (5), 418 (1962).
 - 34 B.J. Baliga, *Modern Power Devices*, John Wiley & Sons, New York, 1987.

- 35 J.D. Parsons, "Synthesis, processing and electron transport studies in β -SiC," *Final Tech. Annual Rept.*, June 1992-May 1993, Naval Air Warfare Center Contract No. N60530-92-C-0123 (8/1993).
- 36 D.K. Ferry, "High field transport in wide band gap semiconductors," *Phys. Rev. B.*, 12 (6), 2361 (1975).
- 37 M. Shinohara, M. Yamanaka, H. Daimon, E. Sakuma, H. Okumura, S. Misawa, K. Endo and S. Yoshida, "Growth of high mobility 3C-SiC epilayers by chemical vapor deposition," *Japanese J. Appl. Phys.*, 27 (3), LA34 (1988).
- 38 W.J. Silva, A. Rosengreen and L.L Marsh, Contract No. F33615-67-C-1328 (12/1967).
- 39 B.W. Wessels and H.C. Gatos, "Electronic properties of epitaxial 6H α - silicon carbide," *J. Phys. Chem. Sol.*, 38, 345 (1977).
- 40 W.E. Nelson, F.A. Halden and A. Rosengreen, "Growth and properties of β -SiC single crystals," *J. Appl. Phys.*, 37, 333 (1966).
- 41 A. Suzuki, A. Ogura, K. Furukawa, Y. Fuji, M. Shigeta and S. Nakajima, "Analysis of temperature dependance of hall mobility of non-doped and nitrogen-doped β -SiC single crystals grown by chemical vapor deposition," *J. Appl. Phys.*, 64 (5), 2818 (1988).
- 42 K. Sasaki, E. Sakuma, S. Misawa, S. Yoshida and S. Gonda, "High temperature electrical properties of 3C-SiC epitaxial layers grown by chemical vapor deposition," *Appl. Phys. Lett.*, 45 (1), 72 (1984).
- 43 J.D. Parsons, A.T. Hunter and D.C. Reynolds, "Characterization of high purity, p-type GaAs grown at atmospheric pressure by MOVPE," *Proc. Int. Symp. GaAs and related compounds*, Karuizawa, Japan, 1985; *Inst. phys. conf. Ser.*, 79, 211 (1986).
- 44 C. Van Opdorp and J. Vrakking, "Avalanche breakdown in epitaxial SiC p-n junctions," *J. Appl. Phys.*, 40 (5), 2320 (1969).
- 45 D.M. Caughey and R.E. Thomas, "Carrier mobilities in silicon empirically related to doping and field," *Proc. IEEE.*, 55, 2192 (1967).

- 46 W. Von Muench and E. Pettenpaul, "Saturated electron drift velocity in 6H α -silicon carbide," *J. Appl. Phys.*, 48 (11), 4823 (1977).
- 47 L. Patrick and W.J. Choyke, "Static dielectric constant of SiC," *Phys. Rev B.*, 2, 2255 (1970).
- 48 G.A. Slack, "Thermal conductivity of pure and impure silicon carbide," *J. Appl. Phys.*, 35 (12), 3460 (1964).
- 49 R.I. Scace and G.A. Slack, "Si-C and Ge-C phase diagrams," *Silicon Carbide, Proc. Conf.*, Boston, Eds. J.R. O'Coonnor, J. Smithens, Pergamon Press, 24 (1960).
- 50 J.S. Blakemore, "Semiconducting and other major properties of gallium arsenide," *J. Appl. Phys.*, 53 (10), R123 (1982).
- 51 *Properties of Si* EMIS Data Review Series No. 4, Published by: INSPEC, the Institution of Electrical Engineers, London and New York, 35 (1988).
- 52 J.A. Lely, "Darstellung von einkristallen von siliziumcarbid und beherrschung von art und menge der eingebauten verunreinigungen," *Ber. Deut. Keram. Ges.*, 32, 229 (1955).
- 53 W.S. Woo, S. Nishino and H. Matsunami, "Polytype change of SiC at high temperature," in *Amorphous and Crystalline SiC II*, Springer Proc. in Phys. 43, 8 (1989).
- 54 J.D. Parsons, G.B. Kruaval and J.A. Vigil, "Beta-SiC on titanium carbide for solid state devices," *Proc. Second International Conf. on Amorphous and Crystalline SiC and Related material*, Santa Clara University, Dec. 15 and 16, 1988, Eds. M.M. Rahman, C.Y. Yang, G.L. Harris, Berlin: Springer-Verlag, 171 (1989).
- 55 A. Addamiano and J.A. Sprague, "Buffer layer technique for the growth of single crystal SiC on Si," *Appl. Phys. Lett.*, 44 (5), 525 (1984).
- 56 S. Nishino and J. Saraie, "Heteroepitaxial growth of cubic SiC on Si substrate using the Si₂H₆-C₂H₂-H₂ system," in *Amorphous and Crystalline SiC and Rel. Materials*; Springer Proc. in Physics., 43, 8 (1989).

- 57 P. Liaw and R.F. Davis, "Epitaxial growth and characterization of β -SiC thin film," *J. Electrochem. Soc.*, 132, 642 (1985).
- 58 H.S. Kong, Y.C. Wang, J.T. Glass, and R.F. Davis, "The effect of off-axis Si (100) substrates on the defect structure and electrical properties of β -SiC thin films," *J. Mater. Res.*, 33, 521(1988).
- 59 I. Golecki, F. Reidinger and J. Marti, "Single crystalline, epitaxial cubic SiC films grown on (100) Si at 750 °C by chemical vapor deposition," *Appl. Phys. Lett.*, 60, 1703 (1992).
- 60 A.J. Steckl and J.P. Li, "Uniform β -SiC thin film growth on Si by low pressure rapid thermal chemical vapor deposition," *Appl. Phys. Lett.*, 50, 203 (1987).
- 61 S.R. Nutt, D.J. Smith, H.J. Kim and R.F. Davis, "Interface structures in β -SiC thin film," *Appl. Phys. Lett.*, 60, 2107 (1992).
- 62 B. Segall, S.A. Alterovitz, E.J. Hauglan and L.G. Matus, "Compensation in epitaxial cubic films," *Appl. Phys. Lett.*, 49, 584 (1986).
- 63 T. Sugii, T. Aoyama and T. Ito, "Low temperature growth of β -SiC on Si by gas-source MBE," *J. Electrochem. Soc.*, 137, 989 (1990)
- 64 K.L. More, H.S. Kong, J.T. Glass and R.F. Davis, "Electron microscopy of defects in epitaxial β -SiC thin films grown on silicon and carbon (0001) faces of α -SiC substrates," *J. Am. Ceram. Soc.*, 73, 1283 (1990).
- 65 H.S. Kong, J.T. Glass and R.F. Davis, "Epitaxial growth of β -SiC thin films on 6H α -SiC substrate via chemical vapor deposition," *Appl. Phys. Lett.*, 49, 1074 (1986).
- 66 Y.C. Wang, J.T. Glass and R.F. Davis, "Effect of substrate orientation on interfacial and bulk character of chemical vapor deposited monocrystalline silicon carbide thin film," *J. Am. Ceram. Soc.*, 73, 1289 (1990).
- 67 H.S. Kong, J.T. Glass and R.F. Davis, "Chemical vapor deposition and characterization of 6H α -SiC thin films on off axis 6H α -SiC substrates," *J. Appl. Phys.*, 64 (5), 2672, (1988).
- 68 T. Ueda, H. Nishino and H. Matsunami, "Crystal growth of SiC by step

- controlled epitaxy," *J. Cryst. Grow.*, 104, 695 (1990).
- 69 J.A. Powell, J.B. Petit, J.H. Edgar, I.G. Jenkins, L.G. Matus, J.W. Yang, P. Pirouz, W.J. Choyke, L. Clemen and M. Yoganathan, "Controlled growth of 3C-SiC and 6H α -SiC," *Appl. Phys. Lett.*, 59 (3), 333 (1991).
- 70 J.A. Powell, D.J. Larkin, J.B. Petit, J.H. Edgar, "Investigation of the growth of 3C-SiC and 6H α -SiC on low tilt angle vicinal (0001) 6H α -SiC wafers," in *Amorphous and Crystalline SiC IV*, Eds. C. Y. Yang, M.M. Rahman and G.L. Harris, Berlin: Springer-Verlag, 23 (1992).
- 71 T. Yoshinobu, H. Mitsui, I. Izumikawa, I. Fuyuki and H. Matsunami, "Lattice matched epitaxial growth of single crystalline 3C-SiC on 6H α -SiC substrates by gas source molecular beam epitaxy," *Appl. Phys. Lett.*, 60, 824 (1992).
- 72 J.D. Parsons R.F. Bunshah and O.M. Stafsudd, "Unlocking the potential of beta silicon carbide," *Sol. St. Tech.*, 28 (11), 133 (1985).
- 73 J.D. Parsons, G.B. Kruaval and J.A. Vigil, " β -SiC on titanium carbide for solid state devices," invited paper, in *Amorphous and Cryst. SiC and Related Materials II*, Ed. Rahman et. al., Berlin: Springer-Verlag, 171 (1989).
- 74 J.J. Bellina in *Amorphous and Cryst. SiC*, Spring Proc. in Phys., Eds. G.L. Harris and C.Y. -W Yang, Berlin: Springer, 43, 162 (1989).
- 75 V. H. Watt and K.H. Jakson, "Au-Ni contacts on beta-SiC films," *Amorphous and Cryst. SiC*, Spring Proc. in Phys., Eds. G.L. Harris and C.Y. -W Yang, 34, 179 (1989).
- 76 P.G. McMullin, J.A. Spitznagel, J.R. Szedon and J.A. Costall in *Proc. ICACSC 90*, Eds. G.L. Harris, M.G. Spencer and C.Y. -W Yang (Washington DC), 294 (1990).
- 77 K.M. Geib, J.E. Mahan and C.W. Wilmsen, "W/SiC contact resistance at elevated temperatures," in *Amorphous and Cryst. SiC and Related Materials II*, Spring Proc. in Phys., Eds. M.M. Rehman, C.Y. Yang and G.L. Harris, 43, 224 (1989).
- 78 K.M. Geib, C. Wilson, R.G. Long and C.W. Wilmsen, "Reaction between SiC and W, Mo, and Ta at elevated temperatures," *J. Appl. Phys.*, 68 (6), 2796

(1990).

- 79 M.M. Anikin, M.G. Rastegaeva, A.L. Syrkin and I.V. Chuiko, *Proc. ICACSC 90*, Eds. M.G. Spencer and C.Y. -W Yang (Washington DC), 191 (1990).
- 80 A.V. Naumov, S.V. Nikitin, A.T. Ostroumov and Yu A. Vodakov, *Fizika i Tekhnika Poluprovodnikov*, 21, 377 (1987).
- 81 D.E. Ioannou, N.A. Papanicolaou and P.E. Nordquist, Jr., "The effect of heat treatment on Au Schottky contacts on β -SiC," *IEEE Trans. Electron Devices*, ED-34, 1694 (1987).
- 82 R.F. Davis, G. Kelner, M. Shur, J.W. Palmour and J.A. Edmond, "Thin film deposition and microelectronic and optoelectronic device fabrication and characterization in monocrystalline alpha and beta silicon carbide," *Proceedings of the IEEE*, 79 (5), 677 (1991).
- 83 *Data in Science and Technology, Semiconductor, Group IV Elements and III-V compounds*, Ed. O. Madelung, Springer-Verlag, Berlin, 47 (1991).
- 84 *Handbook of Chemistry and Properties (CRC), 68th Edition*, Eds. R.C. Weast, M.J. Astle and W.H. Beyer, CRC Press Inc., Boca Raton, FL, (1987-1988).
- 85 L.E. Toth, *Transition Metal Carbides and Nitrides*, Academic Press, New York, (1971).
- 86 D.T. Morelli, "Thermal conductivity and thermo electric power of titanium carbide single crystals," *Phys. Rev. B.*, 44 (11), 5453 (1991).
- 87 J.D. Parsons, " β -SiC power impatt development," *Interim Tech. Annual Rept. 3*, Sept. 1987-Sept. 1988, Naval Weapons Center Contract No. N60530-85-C-0163 (3/1989).
- 88 J.R. Waldrop and R.W. Grant, "Metal schottky barrier contacts to alpha 6H-SiC," *J. Appl. Phys.*, 72 (10), 4757 (1992).
- 89 I. Tamm, *Physik. Z. Sowjetunion*, 1, 733 (1932).
- 90 W. Shockley, *Phys. Rev.*, 56, 317 (1939).

- 91 J. Bardeen, "Surface states and rectification at metal-semiconductor contact," *Phys. Rev.*, 71 (10), 717 (1947).
- 92 J.D. Parsons, "Inverted-vertical OMVPE reactor: design and characterization," *J. Cryst. Growth*, 116, 387 (1992).
- 93 J.D. Parsons, "Method of making ohmic contact structure," U.S. patent No. 4,738,937 (4/19/1988).
- 94 J.D. Parsons, "Electrical contacts to β -SiC" *High Temp. Electronics Workshop*, Albuquerque, N.M., Marriot Hotel (June 6-8, 1989).
- 95 J.D. Parsons, "Single crystal epitaxial growth of β -SiC for device and integrated circuit application," *Mat. Res. Soc. Symp. Proc.*, 97, 271 (1987).
- 96 J.A. Edmond, J. Ryu, J.T. Glass and R.F. Davis, "Electrical contacts to beta silicon carbide thin films," *J. Electrochem. Soc.*, 135, 359 (1988).
- 97 R.C. Glass, L.M. Spellman and R.F. Davis, "Low energy ion-assisted deposition of titanium nitride ohmic contacts on alpha 6H-silicon carbide," *Appl. Phys. Lett.*, 59 (22), 2868 (1991).
- 98 M.I. Chaudhry, W.B. Berry and M.V. Zeller, "Ohmic contacts on β -SiC," *Mat. Res. Soc. Symp. Proc.*, 162, 507 (1990).
- 99 J.J. Bellina Jr. and M.V. Zeller, "Thermally activated reactions of titanium thin films with (100) 3C-SiC substrates," *Novel Refractory Semiconductors*, Eds. D. Emin, T. Aselege and C. Wood, *Mat. Res. Soc. Symp. Proc.*, 97, 265 (1987).
- 100 A. Addamiano, U.S. Patent No. 3,510,733 (5/5/70).
- 101 V.A. Dmitriev, K. Irvine, M. Spencer and G. Kelner, "Low resistivity ($\approx 10^{-6} \Omega \cdot \text{cm}^2$) ohmic contacts to 6H silicon carbide fabricated using cubic silicon carbide contact layer," *Appl. Phys. Lett.*, 64 (3), 318 (1994).
- 102 M.G. Rastegaeva and A.L. Syrkin, "Electrical characteristics of tungsten-contacts to 6H α -SiC at temperatures between 300 and 950 °K," *Sensors and Actuators A*, 33, 95 (1992).
- 103 W. R.L. Lambrecht and B. Segall, "Electronic structure of SiC-TiC interfaces,"

Acta Metall. Mater., 40, S17 (1992).

- 104 H. Daimon, M. Yamanaka, E. Sakuma, S. Misawa and S. Yoshida, "Annealing effects on Al and Al-Si contacts with 3C-SiC," *Jap. J. Appl. Phys.*, 25, (7), L592 (1986).
- 105 D.K. Schroder, *Semiconductor material and device characterization*, John Wiley & Sons, New York, 1990.
- 106 G.K. Reeves and H.B. Harrison, "Obtaining the specific contact resistance from transmission line model measurements," *IEEE Electron Dev. Lett.*, EDL-3, 111 (1982).
- 107 S.S. Cohen, "Contact resistance and methods for its determination," *Thin solid films*, 104, 361 (1983).
- 108 Richard S. Muller, Theodore I. Kamins, *Device Electronics for Integrated Circuits*, Second Ed., John Wiley and Sons, New York.
- 109 W. Shockley, A. Goetzberger and R.M. Scarlett, "Research and investigation of inverse epitaxial UHF power transistors," Rep. No. AFAL-TDR-64-207, Air Force Avionics Lab., Wright-Patterson Air Force Base, OH, Sept. 1964.
- 110 H.H. Berger, "Models for contacts to planar devices," *Solid-state Electron.*, 15, 145 (1972).
- 111 E.G. Woelk, H. Krautle and H. Beneking, "Measurement of low resistive ohmic contacts on semiconductors," *IEEE Trans. Electron Devices*, ED-33 (1), 19 (1986).
- 112 J.S. Shor, R.A. Webber, L.G. Provost, D. Goldstein and A.D. Kurtz, "High temperature ohmic contact metallizations for n-type 3C-SiC," *J. Electrochem. Soc.*, 141 (2), 579 (1994).
- 113 J.D. Parsons, D.A. Roberts, J.G. Wu, A.K. Chaddha, H-S. Chen and H. Hockenhull, "Chemical vapor deposition of beta silicon carbide epilayers using single source precursor 1,2-disilylethane," *MRS Symposia Proceedings*, 282, 463 (1993).
- 114 J.L. Vossen and J.J. Cuomo, "Glow discharge sputter deposition," *Thin Film*

- Processes*, Eds. J.L. Vossen and W.Kern, Academic Press, New York, 12 (1978).
- 115 J.A. Thornton and A.S. Penfold, "Cylindrical magnetron sputtering," *Thin Film Processes*, Eds. J. L. Vossen and W. Kern, Academic Press, New York, 76 (1978).
- 116 D.B. Fraser, "The sputter and S-gun magnetrons," *Thin Film Processes*, Eds. J.L. Vossen and W. Kern., Academic Press, New York, 115 (1978).
- 117 R.K. Waits, "Planar magnetron sputtering," *Thin Film Processes*, Eds. J.L. Vossen and W. Kern, Academic Press, New York, 131 (1978).
- 118 O. Almen and G. Bruce, "Collection and sputtering experiments with noble gas ions," *Nucl. Instrum. methods*, 11 (2), 257 (1961).
- 119 O. Almen and G. Bruce, "Sputtering experiments in the high energy region," *Nucl. Instrum. methods*, 11 (2), 279 (1961).
- 120 L.I. Maissel, in *Handbook of thin film technology*, Ch. 4, Eds. L.I. Maissel and R. Glang, McGraw-Hill, New York, 1970.
- 121 J.L. Vossen, "Control of film properties by RF-sputtering techniques," *J. Vac. Sci. Technol.*, 8 (5), S12 (1971).
- 122 J.W. Coburn and E. Kay, "Plasma diagnostics of an RF-sputtering glow discharge," *Appl. Phys. Lett.*, 18 (10), 435 (1971).
- 123 J.L. Vossen, J.J. O'Neill, K.M. Finlayson and L.J. Royer, "Back-scattering of material emitted from RF-sputtering targets," *RCA Rev.*, 31 (2), 293 (1970).
- 124 *VLSI Technology*, Ed. S.M. Sze, McGraw-Hill book company, New York, 1983.
- 125 D.B. Fraser and H.D. Cook, "Highly conductive, transparent films of sputtered $\text{In}_{2-x}\text{Sn}_x\text{O}_{3-y}$," *J. Electrochem. Soc.*, 119 (10), 1368 (1972).
- 126 J.L. Vossen, "Contamination in films sputtered from hot-pressed targets," *J. Vac. Sci. Technol.*, 8 (6), 751 (1971).
- 127 P. Bacuvier and P. Lavallee, "Some experimental data related to cathodic

- sputtering of powders," *J. Vac. Sci. Technol.*, 13 (5), 1101 (1976).
- 128 L. Holland, "The cleaning of glass in glow discharge," *Br. J. Appl. Phys.*, 9 (10), 410 (1958).
- 129 J.L. Vossen and E.B. Davidson, "Interaction of photoresists with metals and oxides during radio-frequency sputter-etching," *J. Electrochem. Soc.*, 119 (2), 1708 (1972).
- 130 R.P.H. Gasser, "Properties and reactions of clean metal surfaces," *Quart. Rev. Chem. Soc.*, 25 (2), 223 (1971).
- 131 J.E. Houston and R.D. Bland, "Relation between sputter cleaning parameters and surface contaminants," *J. Appl. Phys.*, 44 (6), 2504 (1973).
- 132 G.J. Kominiak and D.M. Mattox, "Reactive plasma cleaning of metals," *Thin Solid films*, 40, 141 (1977).
- 133 A.K. Chaddha, J.D. Parsons and G.B. Kruaval, "Low specific resistance ($\approx 1.3 \times 10^{-5} \Omega \cdot \text{cm}^2$) TiC ohmic contacts to n-type $6H\alpha\text{-SiC}$," *Appl. Phys. Lett.*, 66 (6), 760 (1995).
- 134 J.D. Parsons, G.B. Kruaval and A.K. Chaddha, "Transfer length method characterization of epitaxial and polycrystalline TiC ohmic contacts to (0001) n-type $6H\alpha\text{-SiC}$," to be submitted for publication to *Appl. Phys. Lett.*, 1997.
- 135 J.D. Parsons, G.B. Kruaval and A.K. Chaddha, "Low specific resistance ($\approx 5.44 \times 10^{-6} \Omega \cdot \text{cm}^2$) TiC ohmic contacts to n-type $\beta\text{-SiC}$," *Appl. Phys. Lett.*, 65 (16), 2075 (1994).
- 136 *Data in Science and Technology, Semiconductors, Group IV elements and III-V compounds*, Ed. O. Madelung, Springer-Verlag, Berlin, 1991.
- 137 Q.H. Zhao, J.D. Parsons, H.S. Chen, A.K. Chaddha, J. Wu, G.B. Kruaval and D. Downham, "Single crystal titanium carbide, epitaxially grown on zincblende and wurtzite structures of silicon carbide," *Materials Research Bulletin*, 30 (6), 761 (1995).
- 138 J.D. Parsons, "Vapor phase epitaxy of beta-silicon carbide on titanium carbide," *Ph.D. Dissertation*, UCLA (12/1981).

VITA

The author was born in north-eastern city of Bahraich in state of Uttar Pradesh, India, on Dec. 7, 1966. His early education was completed in Ferozpur, Punjab. He received his B.Tech., Metallurgical Engineering degree from Regional Engineering College, Rourkela, Orissa whereafter he arrived to U.S. for higher education at Oregon Graduate Institute of Science and Technology. During the course of completion of his Ph.D. in Materials Science and Engineering he also secured a M.S., Electrical engineering in field of his interest in Semiconductor processing and devices. All through his Ph.D. he worked as research assistant for Dr. James D. Parsons.

List of publications include:

- 1) "Chemical Vapor Deposition of Beta-SiC films on TiC, using 1,3 Disilacyclo-butane," Applied Physics Letters, 62 (24), 3097 (1993).
- 2) "Thermally stable, low specific resistance ($1.3 \times 10^{-5} \Omega \cdot \text{cm}^2$) TiC ohmic contacts to n-type 6H α -SiC," Applied Physics Letters, 66 (6), 760 (1995).